Aus dem Herzzentrum der Universität zu Köln
Klinik und Poliklinik für Innere Medizin III
Direktor: Universitätsprofessor Dr. med. St. Baldus

Characterization of the murine heart and cardiac macrophages after sepsis

Inaugural-Dissertation zur Erlangung der Doktorwürde
der Medizinischen Fakultät
der Universität zu Köln

vorgelegt von
Charlotte Schreiber
aus Lüneburg, Deutschland

promoviert am 25. März 2025

Gedruckt mit Genehmigung der Medizinischen Fakultät der Universität zu Köln
2025

Dekan: Universitätsprofessor Dr. med. G. R. Fink
1. Gutachter: Privatdozent Dr. med. F. F. Hoyer
2. Gutachter: Privatdozent Dr. med. F. Nguemo

Erklärung

Ich erkläre hiermit, dass ich die vorliegende Dissertationsschrift ohne unzulässige Hilfe Dritter und ohne Benutzung anderer als der angegebenen Hilfsmittel angefertigt habe; die aus fremden Quellen direkt oder indirekt übernommenen Gedanken sind als solche kenntlich gemacht.
Bei der Auswahl und Auswertung des Materials sowie bei der Herstellung des Manuskriptes habe ich Unterstützungsleistungen von folgenden Personen erhalten:

PD Dr. Friedrich Felix Hoyer
Herr Simon Geißen

Weitere Personen waren an der Erstellung der vorliegenden Arbeit nicht beteiligt. Insbesondere habe ich nicht die Hilfe einer Promotionsberaterin/eines Promotionsberaters in Anspruch genommen. Dritte haben von mir weder unmittelbar noch mittelbar geldwerte Leistungen für Arbeiten erhalten, die im Zusammenhang mit dem Inhalt der vorgelegten Dissertationsschrift stehen.

Die Dissertationsschrift wurde von mir bisher weder im Inland noch im Ausland in gleicher oder ähnlicher Form einer anderen Prüfungsbehörde vorgelegt.

Die in dieser Arbeit angegebenen Experimente sind nach entsprechender Anleitung durch Herrn Simon Geißen von mir selbst ausgeführt worden, sofern im folgenden Methodenteil nicht anders gekennzeichnet.
Ein kleiner Teil dieser der Dissertationsschrift zugrunde liegenden Experimente sind von mir in Zusammenarbeit mit Herrn Jordi Hees Soler durchgeführt worden und die Ergebnisse bereits in seiner Bachelorarbeit genutzt worden (Figure 3.1). Zum besseren Verständnis sind diese Auswertungen auch in dieser Arbeit aufgeführt und mit Hinweisen auf Herrn Hees Solers Bachelorarbeit gekennzeichnet.

Die CLP-Operationen an den Versuchstieren wurden zum Teil von Herrn Simon Geißen und zum Teil von mir selbst nach Anleitung durch Simon Geißen durchgeführt.

Erklärung zur guten wissenschaftlichen Praxis:

Ich erkläre hiermit, dass ich die Ordnung zur Sicherung guter wissenschaftlicher Praxis und zum Umgang mit wissenschaftlichem Fehlverhalten (Amtliche Mitteilung der Universität zu Köln AM 132/2020) der Universität zu Köln gelesen habe und verpflichte mich hiermit, die dort genannten Vorgaben bei allen wissenschaftlichen Tätigkeiten zu beachten und umzusetzen.

Köln, den 02.10.2024

Unterschrift:

Danksagung

Besonders bedanken möchte ich mich bei meinem Betreuer, Simon Geißen, der mich in das Experimentelle Arbeiten eingeführt hat und mit seinem ausführlichen Fachwissen zu Methodik und wissenschaftlichem Hintergrund jederzeit ein sehr wertvoller Ansprechpartner war. Mit seinen kritischen Rückfragen und Ermutigungen hat er mich durch den gesamten Entstehungsprozess der Dissertation geführt und damit diese Arbeit erst möglich gemacht.
Ebenso gilt mein Dank meinem Doktorvater, PD Dr. Friedrich Felix Hoyer für die Bereitstellung des Themas. Seine Expertise und stets zugewandte Unterstützung waren mir eine große Hilfe.
Bei der AG Baldus und der AG Winkels der Klinik III für Innere Medizin der Universität zu Köln bedanke ich mich ebenfalls für die ständige Hilfsbereitschaft, den Austausch und die Unterstützung im Rahmen der experimentellen Arbeit und für die kritischen Diskussionen. Besonders hervorheben möchte ich dabei Simon Grimm und Dr. Alexander Hof.
Außerdem gilt mein Dank den Graduiertenprogrammen TRR 259 und Cologne Cardiovascular Research Center (CCRC) der Deutschen Forschungsgemeinschaft (DFG) für ihre ideelle und finanzielle Unterstützung. Die verschiedenen Workshops und Vorträge halfen mir, mein Wissen zu vertiefen und in der Diskussion mit den anderen Graduierten meine eigene Arbeit zu verbessern. Mein besonderer Dank gilt Leoni Feik für ihre Unterstützung beim Erlernen des Schneidens und Färbens von histologischen Präparaten.

TABLE OF CONTENTS

LIST OF ABBREVIATIONS 7

1. SUMMARY 10

1.1 Summary (English) 10

1.2 Zusammenfassung (Deutsch) 11

2. INTRODUCTION 12

2.1 Sepsis 12

2.1.1. Pathophysiology of sepsis 12

2.1.2. Sepsis and the concepts of trained immunity and endotoxin tolerance 14

2.1.3. Murine sepsis models 15

2.2 Chemotaxis of neutrophils 16

2.3 Aims 17

3. MATERIAL AND METHODS 19

3.1 Animal model 19

3.1.1. Anesthesia and narcosis 19

3.1.2. CLP surgery 19

3.1.3. Blood collection 20

3.1.4. Echocardiography 21

3.1.5. Organ harvesting 22

3.2 Molecular biological methods 23

3.2.1. Real time qPCR 23

(1) RNA-Isolation 23

(2) Reverse Transcription 23

(3) Realtime PCR (using Taq®Man Assay) 23

(4) Realtime PCR (using GoTaq® qPCR Master Mix) 23

3.2.2. SDS-Page and Western Blot 25

(1) Protein isolation 25

(2) BCA-Assay 25

(3) SDS-PAGE 25

(4) Western Blot 25

3.3 Histological methods 26
3.3.1. Cryosections 26
(1) H&E-Staining 26
(2) Picrosirius Red Staining 27
3.3.2. Paraffin sections 27
(1) H&E-Staining 28
(2) Picrosirius-Red Staining 28

3.4 Single-cell RNA sequencing 28
3.4.1. Organ harvest and sample preparation 29
3.4.2. Single-cell RNA sequencing 31

3.5 Statistical analyses 31
3.5.1. T-test 31
3.5.2. ANOVA 32

4. RESULTS 34

4.1 Immune response after CLP 34

4.2 Heart function after CLP 36

4.3 Heart morphology after CLP 39

4.4 Single-cell RNA sequencing of cardiac macrophages 43

5. DISCUSSION 45

5.1 Chronic effects of sepsis 45

5.2 Sepsis does not lead to chronic changes in murine heart function and morphology. 46

5.3 Sepsis chronically impacts the macrophage milieu of the murine heart. 47

5.4 Limitations 48

5.5 Conclusion 49

6. REFERENCES 50

7. APPENDIX 56

7.1 List of Figures 56

7.2 List of Tables **56**

7.3 Recipes **57**

7.3.1. RIPA-Buffer 57

7.3.2. 4x Laemmli Sample Buffer 57

7.3.3. 10x SDS-PAGE Running Buffer 57

7.3.4. Transfer Buffer 57

7.4 Supplementary Figures **58**

7.4.1. Original Pictures WesternBlot 58

7.4.2. Pathways enrichment analysis of cluster 5 60

7.4.3. Unpaired samples t-test of Fractional Shortening 7 weeks after CLP 60

List of Abbreviations

A: Ampere

APC: Allophycocyanin

Aq. dest.: Destilled water

ARDS: Acute respiratory distress syndrome

BCA: Bicinchoninacid

BCG: Bacillus Calmette-Guérin

BNP: Brain natriuretic peptide

BSA: Bovine serum albumine

BW: Bodyweight

C: Celsius

C3a: Complement component 3a

C5a: Complement component 5a

CCL2: C-C Motif Chemokine Ligand 2

CCL8: C-C Motif Chemokine Ligand 8

CCL12: C-C Motif Chemokine Ligand 12

CCR2: C-C Motif Chemokine Receptor 2

CD: Cluster of differentiation

cDNA: Complementary DNA

CLP: Cecal ligation and puncture

cm: Centimeter

Col1a1: Collagen Type I Alpha 1 Chain

Col3a1: Collagen Type III Alpha 1 Chain

CXCL1: C-X-C Motif Chemokine Ligand 1

CXCL2: C-X-C Motif Chemokine Ligand 2

CXCR2: C-X-C Motif Chemokine Receptor 2

CXCR4: C-X-C Motif Chemokine Receptor 4

CXR Reference Dye: Carboxy-X-Rhodamine Reference Dye

d: Day

DAMPs: Danger-associated molecular patterns

DIC: Disseminated intravascular coagulation

DNA: Desoxyribonucleinacid

DTT: Dithiothreitol

EDTA: Ethylenediaminetetraacetic acid

e.g.: exempli gratia; for example

ELISA: Enzyme-linked Immunosorbent Assay

ERK1: MAPK3; Mitogen-activated protein kinase 3

ERK2: MAPK1; Mitogen-activated protein kinase 1
FACS: Fluorescence activated cell sorting
FBS: Fetal bovine serum
FITC: Fluorescein isothiocyanate
g: Gram
GAPDH: Glyceraldehyde 3-phosphate dehydrogenase
G-CSF: Granulocyte colony-stimulating factor
h: Hour
HCl: Hydrochloric acid
HE-staining: Hematoxylin and eosin staining
i.p.: Intraperitoneal
IL-1: Interleukin 1
IL-1β: Interleukin-1β
IL-6: Interleukin-6
IL-10: Interleukin-10
IU: International unit
i.v.: Intravenous
kDa: Kilodalton
kg: Kilogram
LPS: Lipopolysaccharide
MetOH: Methanol
mg: Milligram
MIP-2: Macrophage inflammatory protein 2
ml: Milliliter
mM: Millimolar
mmHg: Millimeter of mercury
mmol/L: Millimole per liter
mRNA: Messenger ribonucleic acid
NaCl: Sodium chloride
n: Number of animals
NETs: Neutrophils extracellular traps
ng: Nanogram
nm: Nanometer
OCT-Compound: Optimal cutting temperature compound
PAI-1: Plasminogen-activator-inhibitor 1
PAMPs: Pathogen-associated molecular patterns
PBS: Phosphate buffer saline

PCR: Polymerase chain reaction

PE: Phycoeryhrin

PFA: Paraformaldehyde

PRRs: Pattern recognition receptors

qPCR: Quantitative polymerase chain reaction

quickSOFA score: Quick Sepsis-related organ failure assessment score

rcf: Relative centrifugal force

RIPA: Radio Immuno Precipitation Assay

RNA: Ribonucleic acid

ROS: Reactive oxygen species

Rpm: Rounds per minute

s: Second

S100a8: S100 calcium binding protein A8

S100a9: S100 calcium binding protein A9

s.c.: Subcutaneous

SDS: Sodium dodecyl sulfate

SDS-PAGE: Sodium dodecyl sulfate polyacrylamide gel electrophoresis

SIRS: Systemic inflammatory response syndrome

Socs3: Suppressor of Cytokine Signaling 3

TBS/T: Tris-buffered saline with Tween20

TGFβ: Transforming growth factor β

TLR4: Toll-like receptor 4

TNF: Tumor necrosis factor

TNF-α: Tumor necrosis factor α

TREM2: Triggering receptor expressed on myeloid cells 2

TTC: 2,3,5-Triphenyl-tetrazolium chloride

UMAP: Uniform Manifold Approximation and Projection

UNG: Uracil-DNA glycosylase

V: Volt

x: Times

µl: Microliter

°: Degree

%: Percent

1. Summary

1.1 Summary (English)

Sepsis is a severe disease that is characterized by a dysregulated host immune response to infection. Even after surviving the life-threatening acute complications, sepsis patients suffer from long-term consequences including a higher risk for cardiovascular events like acute myocardial infarction. The aim of this thesis is to investigate what chronic changes are triggered by sepsis in the murine heart and in tissue resident cardiac macrophages.

Cecal Ligation and Puncture (CLP) was used to model sepsis in mice. CLP leads to an increase of blood neutrophils for about 6 weeks. Male and female mice show baseline differences in blood leukocyte count and distribution but react similarly to sepsis with leukocytosis and neutrophilia.

Systolic and diastolic heart function and BNP expression in cardiac tissue are not altered seven weeks after CLP, so there is no evidence of impaired cardiac function. Cardiac morphology is also not chronically altered after CLP: There are no signs of cardiac hypertrophy in the histological or echocardiographic analyses. Furthermore, there is no evidence of cardiac fibrosis, as neither an increase in the proportion of fibrosis is observed histologically nor a change in the expression of fibrosis-inducing genes.

However, single-cell RNA sequencing reveals a previously unknown cardiac macrophage population after sepsis. This cluster displays prominent inflammatory features. Specifically, genes that drive the attraction of inflammatory leukocytes are upregulated.

Whether this newly discovered macrophage population contributes to cardiovascular morbidity and mortality after sepsis is not yet known. Future studies are needed to determine this populations functional relevance.

1.2 Zusammenfassung (Deutsch)

Sepsis ist eine schwere Erkrankung, die durch eine gestörte Immunreaktion des Wirts auf eine Infektion gekennzeichnet ist. Selbst nach dem Überleben der lebensbedrohlichen akuten Komplikationen leiden Sepsis-Patienten an Langzeitfolgen, darunter ein erhöhtes Risiko für kardiovaskuläre Ereignisse wie Myokardinfarkte. Ziel dieser Arbeit ist es, zu untersuchen, welche chronischen Veränderungen durch eine Sepsis im Herzen und insbesondere in den gewebeansässigen Herzmakrophagen ausgelöst werden.

In dieser Arbeit wurde zur Modellierung von Sepsis in Mäusen das Zökum ligiert und punktiert (CLP). Die CLP-Operation führt zu einem Anstieg der neutrophilen Granulozyten im Blut für etwa 6 Wochen. Männliche und weibliche Mäuse zeigen vor dem Eingriff Unterschiede in Leukozytenzahl und -verteilung im Blut, reagieren aber in ähnlicher Weise mit Leukozytose und Neutrophilie auf die Sepsis.

Die systolische und diastolische Herzfunktion sowie die BNP-Expression im Herzgewebe sind 7 Wochen nach CLP nicht verändert, sodass es keinen Hinweis auf eine Beeinträchtigung der Herzfunktion gibt. Auch die Herzmorphologie ist nach CLP nicht chronisch verändert: Es gibt keine Anzeichen für eine Herzhypertrophie in den histologischen und echokardiographischen Analysen. Außerdem gibt es keine Hinweise auf eine kardiale Fibrose, da weder histologisch eine Zunahme des Fibroseanteils im Herzen noch eine Veränderung der Expression von Fibrose-induzierenden Genen zu beobachten ist.

Single-cell RNA Sequencing zeigt jedoch eine bisher unbekannte kardiale Makrophagenpopulation nach Sepsis, welche durch pro-inflammatorische Merkmale gekennzeichnet ist. Insbesondere sind Gene für Zytokine, welche für das Anlocken von Leukozyten verantwortlich sind, hochreguliert.

Ob diese neu entdeckte Makrophagenpopulation zur kardiovaskulären Morbidität und Mortalität nach Sepsis beiträgt, ist noch nicht bekannt. Zukünftige Studien sind erforderlich, um die funktionelle Bedeutung dieser Population zu untersuchen.

2. Introduction

2.1 Sepsis

Sepsis is a life-threatening organ dysfunction caused by a dysregulated host response to infection.[1] Over the last decades there was a decrease in the incidence of sepsis of 37% and sepsis mortality of 52.8%. Sepsis is nonetheless still highly relevant, as in 2017 there were 48.9 million sepsis cases worldwide that were responsible for 11 million sepsis-related deaths, representing 19.7% of global deaths.[2]

Sepsis is mainly caused by infections but can also be caused by injuries or other non-communicable diseases such as maternal disorders (for example ectopic pregnancy). In 2017, the leading infectious causes worldwide of sepsis were diarrheal diseases and lower respiratory infections.[2]

Since the fast application of antibiotics significantly improves prognosis, screening of patients for sepsis is highly important.[3] For fast evaluation the quickSOFA score - consistent of three criteria (respiratory rate ≥22, Glasgow Coma Score <15, and systolic blood pressure ≤100 mmHg) - was developed.[1] However, this score should not be used as a single screening tool due to its low sensitivity, even if it may be helpful for a clinician to be alerted to a patient's critical situation and the possibility of sepsis.[3]

Patients with sepsis should be treated at the intensive care unit and immediately given antibiotics, ideally after obtaining 2 sets of peripheral blood cultures.[3,4] If a patient with sepsis requires (despite adequate fluid resuscitation) vasopressors to maintain a mean arterial pressure ≥65 mmHg and shows serum lactate levels >2 mmol/L, he fulfills the diagnosis criteria of septic shock, which correlates with higher mortality than sepsis alone.[1]

Even after surviving sepsis, 63% of patients are re-hospitalized within 1 year after the disease.[5] The risk of mortality and cardiovascular events is elevated in sepsis survivors.[6–13] While various studies agree on the elevated risk of cardiovascular events including ischemic stroke and acute myocardial infarction after sepsis, some find an increased risk also for myocardial infarction alone while others detect no difference in the post-sepsis incidence of myocardial infarction.[8,11–13]

2.1.1. Pathophysiology of sepsis

Acute inflammation is mainly mediated by the innate immune system and can be triggered by microbial infection as in sepsis or by tissue damage. Via pattern recognition receptors (PRRs) macrophages and dendritic cells recognize pathogen-associated molecular patterns (PAMPs) and danger-associated molecular patterns

(DAMPs). The activation of PRRs triggers an intracellular cascade that leads to the production of proinflammatory cytokines and chemokines, such as TNF-α (Tumor necrosis factor α), IL-1β (Interleukin-1β) and IL-6 (Interleukin-6).[14]

In sepsis, simultaneously to this proinflammatory reaction, anti-inflammatory cytokines such as IL-10 (Interleukin-10), TNF soluble receptors and IL-1 receptor antagonist are released and elevation of both types of cytokines predicts mortality. That contrasts with earlier beliefs that defined sepsis as a continuum of pro- and anti-inflammatory reactions.[15]

One example for a PAMP is Lipopolysaccharide (LPS), a component of the outer membrane of gram-negative bacteria. In tissue-resident macrophages it activates via Toll-like Receptor 4 (TLR4) a cascade that causes the production of cytokines such as CXCL1 and CXCL2 (C-X-C Motif Chemokine Ligand 1 and 2). These chemo attractants lead to a transmigration of neutrophils into the inflamed tissue where they fight the bacteria via phagocytosis, degranulation and formation of neutrophil extracellular traps (NETs).[16,17] On the one hand these mechanisms like NET formation are necessary to clear the pathogen from the body, on the other hand they can create tissue-damage and participate in organ failure.[18] While fighting the pathogen invasion, antigen presenting cells of the innate immune system activate T and B cells and thereby the slower adaptive immune response.[19]

Besides cells of the innate and adaptive immunity, the dysregulation of different intertwined systems contributes to the evolution of sepsis: endothelial and microvascular function, coagulation and complement system.[20] The cytokine storm in sepsis activates the endothelial cells and results in dysregulated vascular tone and homeostasis which impairs the vascular barrier. The vascular leak resulting of this mechanism causes tissue edema and can lead to acute respiratory distress syndrome (ARDS), one of the severe complications of sepsis. The endothelial injury causes the release of Tissue Factor that triggers hypercoagulability and can lead to another severe complication: Disseminated intravascular coagulation (DIC). Due to massive formation of microthrombi, microvascular dysfunction, and disordered leukocyte sequestration, the delivery of oxygen to tissue is impaired resulting in lactate acidosis and necrosis. The consumption of thrombocytes results in a reduced platelet count in septic patients.[20] The complement system is also dysregulated in sepsis. It contributes to the proinflammatory response and increases leukocyte recruitment.[20] Different components of the complement system play opposing roles. While C5a exacerbates sepsis via neutrophil activation, C3a is protective via macrophage activation.[21]

Not only pro-inflammatory but also immunosuppressive mechanisms contribute to the pathophysiology of sepsis and can lead to life-threatening secondary infections.[22–24] Sepsis causes apoptosis of multiple immune cells: $CD4^+$-T lymphocytes, B lymphocytes and dendritic cells.[25,26] In monocytes, the presence of apoptotic cells increases the secretion of the anti-inflammatory cytokine IL-10 and decreases the secretion of pro-inflammatory cytokines like TNF-α and IL-1.[27] The coordination of the adaptive immune response is dysregulated. The balance between Th2 and Th1 cells is tilted to a dominance of Th2 cells resulting in a higher perceptibility for secondary infections and higher mortality.[28] Leukocytes from patients with severe sepsis lose their ability to produce cytokines due to defects in the cellular energy metabolism which causes immunoparalysis.[29]

In conclusion, sepsis is a complex disease in which a trigger leads to a cascade that disrupts homeostasis of different systems resulting in a life-threatening disorder. Even if the understanding of the disease increases, the only therapeutic options are still antibiotic treatment of the infection and supportive treatment with fluids and vasoactive agents such as norepinephrine.[3] All clinical trials for immunotherapy in sepsis have failed (excluding the administration of corticosteroids)[3], despite promising results in preclinical studies.[30]

2.1.2. Sepsis and the concepts of trained immunity and endotoxin tolerance

The adaptive immune system has well established specific memory-mechanisms and contrary to earlier assumptions, the innate immune system also has memory functions, albeit unspecific.[31]

The concept of trained immunity was first established in 2011 when Netea et al. proposed this term to describe immunological memory in innate immune cells.[32] The Bacillus Calmette-Guérin (BCG) vaccine against tuberculosis is associated with a better long-term survival during 40 years when administered in childhood and shows in a randomized placebo-controlled phase III trial a significant reduction of new infections in the elderly 1 year after vaccination.[33,34] This unspecific protection against infections is also observed in response to other stimuli such as β-Glucan. It is due to epigenetic reprogramming and metabolic changes in cells of the innate immune system, mainly studied in monocytes.[35–38] While trained immunity can protect against severe infections, it also can have adverse effects due to an overly activated immune system, leading for example to increased atherosclerosis.[31]

Another concept of immunological memory in innate immune cells is endotoxin tolerance. Pretreatment with the endotoxin LPS attenuates the pro-inflammatory

response to a subsequent challenge with LPS.[39] This endotoxin tolerance is also based on epigenetic reprogramming and metabolic changes.[31,40,41] In sepsis, endotoxin tolerance of monocytes contributes to immunosuppression and is associated with the severity of sepsis and organ dysfunction.[42,43] On the other hand, in early stages of sepsis, where the pro-inflammatory reaction dominates, endotoxin tolerance can be protective and some studies show that even if the cytokine production is attenuated, endotoxin tolerance can cause a higher antimicrobial activity and improved survival.[31,44–46]

Adding to the complexity of these mechanisms, the reaction of the innate immune system to endotoxin can be dose dependent.[47,48] Preconditioning mice with super low-dose LPS leads to trained immunity and increased mortality after sepsis while preconditioning with low-dose LPS leads to endotoxin tolerance and decreased mortality.[48]

Trained immunity was first discovered in circulating monocytes which explains immunological memory for up to a week due to the lifespan of monocytes.[31] But as the effects of BCG-vaccination last for decades, it was soon discovered that bone marrow progenitor cells can also be trained.[31,33,49] Recently, trained immunity was also found in tissue-resident macrophages, especially in alveolar macrophages.[50,51] However, not much is known about if and how cardiac tissue-resident macrophages can be trained and this thesis investigates the chronic effects of sepsis on cardiac macrophages.

2.1.3. Murine sepsis models

As sepsis is complex and heterogeneous, there are different sepsis models to mimic the disease in mice. One model is injection of the endotoxin LPS. This model is simple, highly controlled, and standardized but the organism reacts in some respects differently than in human sepsis: After injecting a lethal dose of LPS, cytokines show a high, rapid, and transient increase whereas in sepsis this increase is slower and lasts longer.[52] On the other hand, injecting sublethal doses of LPS into mice primes monocytes to a immunosuppressed status called LPS tolerance, which is similar to the often occurring post-septic immunosuppression.[53] Another model is the inoculation of bacteria in the murine organism, which again underrepresents the complexity of sepsis, as sepsis is often polymicrobial.[54] In this thesis the sublethal Cecal Ligation and Puncture (CLP) model is chosen: The intestinal barrier in the cecum is damaged and the mouse gut bacteria cause a peritonitis. It has a higher variability than the LPS model due to a more complex procedure but mimics the human reaction to sepsis better: the cytokine release,

hemodynamic and metabolic reactions, and dysregulated immune response including post-septic immunosuppression are similar to human sepsis.[52,53]

2.2 Chemotaxis of neutrophils

In sepsis the innate immune system plays a key role. To explain how the innate immune cells are guided to the focus, this section explains the underlying chemotactic processes, focusing on neutrophils and the role of the chemokine CXCL2.

In 1989, Wolpe et al. discovered a chemokine that is produced by macrophages upon stimulation with LPS and attracts human polymorphonuclear leukocytes, nowadays called granulocytes (including neutrophils, eosinophils, and basophils). They named it chemokine macrophage inflammatory protein 2 (MIP-2).[55] Later it was renamed in C-X-C Motif Chemokine Ligand 2 (CXCL2) and it was discovered that this chemoattractant is also produced by endothelial cells[56] and by neutrophils itself leading to a positive feedback cycle and a potent attraction of neutrophils. It regulates neutrophil effector functions, too: it enhances phagocytosis and the production of reactive oxygen species (ROS).[57,58] CXCL2 and the related chemokine CXCL1 procure their effects through the same receptor: C-X-C Motif Chemokine Receptor 2 (CXCR2); but the effector cells respond differently to each chemokine.[58] In peritoneal macrophages stimulated with LPS, the production of CXCL1 and CXCL2 peaked after 1-2 hours and decreased to baseline 4 hours after stimulation. CXCL2 alone results in neutrophil recruitment but the presence of CXCL1 is necessary to maximize the influx.[16]

Infection or tissue damage stimulate the attraction and extravasation of neutrophils to the focus. That leads to an increased demand for generation and mobilization of neutrophils in the bone marrow. CXCL1 and CXCL2 activate CXCR2 in the bone marrow and thereby facilitate the egress of neutrophils into the bloodstream.[59] The pro-inflammatory cytokine Granulocyte colony-stimulating factor (G-CSF) inhibits CXCR4, which normally retains neutrophils in the bone marrow and thereby contributes to neutrophilia.[59–61] On the other hand, in the very early phase of inflammation G-CSF inhibits CXCR2 and thereby prevents excessive neutrophil mobilization.[62]

The neutrophils in the blood stream need to be directed to the focus. In necrotic injury they are guided by an intravascular chemokine gradient of CXCL2 with rising concentrations of CXCL2 in direction to the injury. If neutrophils are CXCR2-deficient or CXCL2 is inhibited with antibodies, this process does not work and the neutrophils migrate randomly.[63] Once in the postcapillary venules near the focus,

neutrophils enter the tissue, which involves an adhesion cascade and finally transmigration. These processes are mediated via different chemokines, selectins and integrins.[64]

2.3 Aims

A better understanding of the complex immune response in sepsis is crucial to the development of therapies for the disease and its consequences. The aim of this thesis is to contribute to this by investigating the effects of sepsis on the heart.

In 2019, Hoyer et al. discovered that after CLP the number of tissue-resident macrophages in the heart increases along with the recruitment of circulating monocytes into the heart (2.5% recruited cells of all tissue-resident macrophages in steady state increases to 6.2% in sepsis). These numeric changes return to baseline after about 63 days. Additionally, 4 days after CLP the expression of different inflammatory genes in cardiac macrophages, both resident and recruited, such as *CCL8* (C-C Motif Chemokine Ligand 8) and IL10, is elevated. They show that these changes may result in protection of the heart during sepsis as a deletion of IL10 from macrophages leads to an increase of blood troponin levels and cardiomyocyte apoptosis after CLP.[65]

It has been shown in various studies, that sepsis survivors show an increased mortality rate and a higher risk for cardiovascular events including myocardial infarction.[7–10] Also the adverse long-term effects of sepsis on atherosclerosis and the central nervous system in mice have been shown.[66,67]

Given the alteration of cardiac resident macrophages during sepsis and the organism-wide long-term alterations caused by sepsis, the aim of this thesis is to investigate the long-term effects of a sublethal sepsis to the murine heart. Specifically, heart function, cardiac morphology, and the RNA expression of heart-resident macrophages were analyzed 7 weeks after CLP.

Hypothesis 1:

H0: Sepsis does not lead to chronic changes in the murine heart function.

H1: Sepsis leads to chronic changes in the murine heart function.

Hypothesis 2:

H0: Sepsis does not lead to chronic changes in the heart morphology.

H1: Sepsis leads to chronic changes in the heart morphology.

Hypothesis 3:

H0: Sepsis does not lead to chronic changes in the macrophage milieu of the murine heart.

H1: Sepsis leads to chronic changes in the macrophage milieu of the murine heart.

3. Material and Methods

Figure 4.1 providing graphical overview was designed using BioRender.

3.1 Animal model

This study exclusively used C57BL/6J mice which were provided partly by local breeding in the Center for Molecular Medicine Cologne (CMMC) and partly by European breeding facilities of Charles River (Wilmington, MA, USA). The animals were transferred to an animal facility in close proximity to our laboratory (Dezentrales Tierhaltungsnetzwerk, Tierhaltung LFI). All the animal experiments were performed according to the FELASA guidelines and are part of the animal testing permission 81-02.04.2020.A253.

3.1.1. Anesthesia and narcosis

At least 30 minutes before performing any surgery or organ harvest the mice were anesthetized with buprenorphine s.c. (0.1 mg/kg BW, injection volume: 10ml/kg BW). For surgeries, i.v. injections and echocardiography the mice were placed under inhalative narcosis with isoflurane (initial dose 5%, maintenance dose 2%). Only for embedding the total heart in paraffine a different narcosis was used: The mice were injected i.p. with an injection narcosis (100µl/10g BW; Table 3.1).
For all surgeries and echocardiography, the mice were placed onto a warming pad and body temperature was constantly measured via a rectal thermometer.

Drug	Purpose	Concentration
Fentanyl	Analgesia	0.05mg/kg BW
Midazolam	Narcosis	5mg/kg BW
Medetomidin	Analgesia/narcosis	0.25mg/kg BW

Table 3.1: Recipe for injection narcosis

3.1.2. CLP surgery

The CLP (cecal ligation and puncture) surgery induces bacterial peritonitis and, subsequently, sublethal systemic immune reaction. The procedure is often described as a lethal sepsis model with survival as a primary endpoint;[68,69] mortality can be modified by adjustment of the procedure to further investigate other endpoints such as organ dysfunction.[70,71]
Laparotomy was performed and the cecum exteriorized and ligated (yarn: EthilonTM Polyamide 6 5-0; Figure 3.2, A-E). In our model, the ligation length was identified as the most important parameter to influence the survival which was shown in an exploratory pilot study performed by Simon Geißen (Figure 3.1) and

has already been shown in rodents.[71,72] As this study aimed to facilitate CLP as a model of barely sublethal sepsis, a ligation length of 0.5 cm was chosen for consecutive experiments.

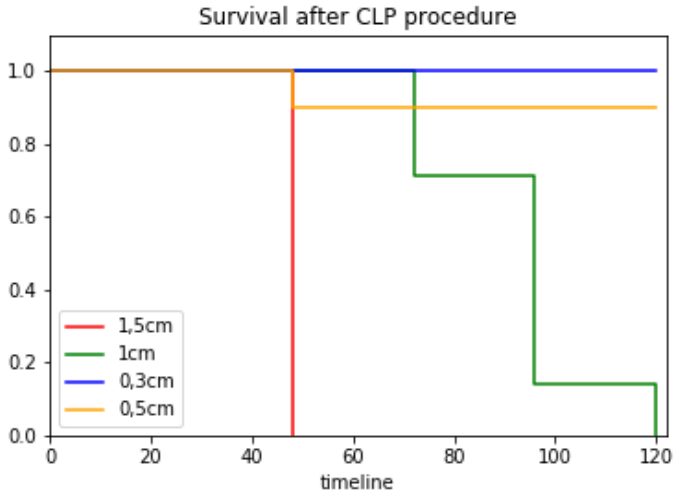

Figure 3.1: Survival after CLP surgery according to ligation length
n=8,7,5,9; survival in hours, ligation length in cm. This data is already shown by Jordi Hees-Soler.[73]

The ligated cecum was punctured with a 30G cannula (Sterican® 0.30x12mm) and relocated to the peritoneum while squeezing the feces into the abdominal cave (Figure 3.2, F). The peritoneum and the skin cuts were sewn (Yarn: Prolene™ Polypropylen -0). To rinse the peritoneal cave, 0.5 ml NaCl 0.9% were injected i.p. Postoperatively, the mice were placed on a warming pad until waking up from the narcosis. For 3 days after surgery the mice received 2 daily i.p.-injections of buprenorphine. The CLP surgeries were performed partly by Simon Geißen and partly by me.

3.1.3. Blood collection

Blood samples were collected by Simon Geißen via cheek punch of the submandibular vein in an EDTA coated tube (Minicollect® 1ml K3 EDTA). I then analyzed the blood in a veterinary hematology analyzer (Element HT5 by Heska).

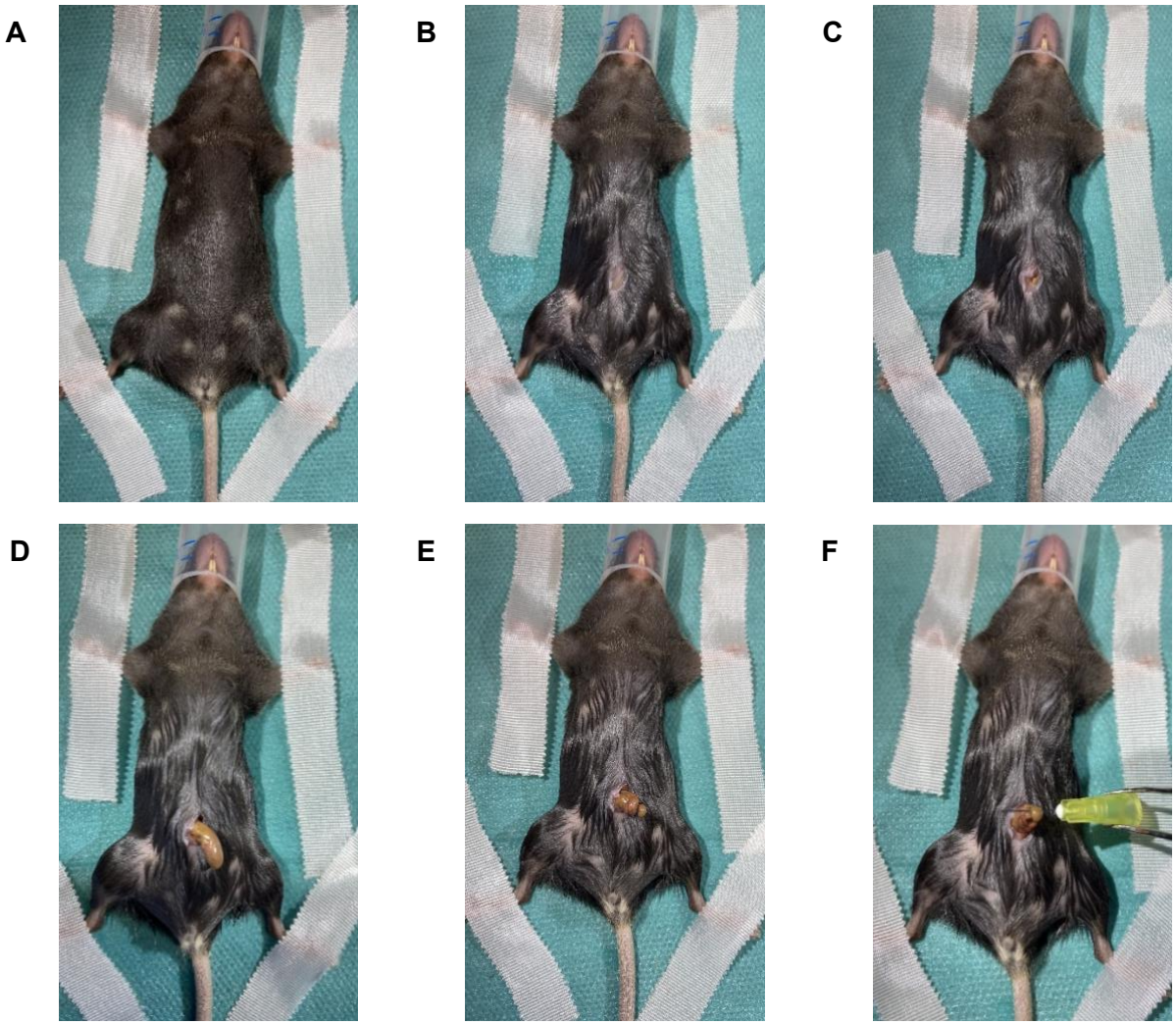

Figure 3.2: Procedure of CLP surgery

A) The mouse is put under narcosis and the abdominal area is disinfected; B) The skin in the lower abdomen is cut longitudinally; C) The peritoneum is incised following the linea alba; D) The cecum is located and exteriorized; E) The cecum is ligated with a ligation length of 0.5cm; F) The ligated part is punctured.

3.1.4. Echocardiography

For the transthoracic echocardiography, a Vevo 3100 ultrasound imaging system and a MX550D transducer were used. Different recordings of the murine heart were taken: Parasternal long-axis view (PSLAX) of the left ventricle in B-Mode and M-Mode, Parasternal short-axis view (SAX) of the left ventricle in B-Mode and M-Mode, Pulsed Wave Doppler (PW-Doppler) images of the mitral valve, and Tissue Doppler images of the mitral valve. The echocardiographies were performed by Simon Geißen.

The analyses of the echocardiographies were performed with VevoLab Software (FujiFilm, VisualSonics). In the PSLAX B-Mode the endocardium was traced end

diastolic and end systolic either by Auto-LV-function or manually if the Auto-LV would not trace the real endocardium. This tracing was used to calculate different parameters of left ventricular function: Stroke Volume [µl] is the blood volume that is ejected in systole; End diastolic Volume (EDV, [µl]) is the left ventricular blood volume at the end of a diastole; Ejection Fraction [EF, [%]) is the Stroke Volume as a fraction of the EDV; Cardiac Output [ml/min] is the Stroke Volume multiplicated with the heart frequency.

The Left Ventricular Posterior Wall thickness in diastole (LVPWd) was measured in M-Mode of PSLAX an SAX and the mean was calculated. LVPWd is a parameter for cardiac hypertrophy.

The PW-Doppler was used to measure the E-wave (peak velocity blood flow in early diastole; caused by ventricle relaxation), the A-wave (peak velocity blood flow in late diastole; caused by atrial contraction) and isovolumetric relaxation time. The Tissue Doppler was used to measure e'-wave (passive movement of mitral annulus; caused by ventricle relaxation) and a'-wave (active movement of mitral annulus; caused by atrial contraction). Out of these values different parameters for left ventricular diastolic function were calculated: E/A (used to evaluate left ventricular filling), E/e' (equivalent to left ventricular end diastolic pressure) and e'/a' (in advanced states of diastolic dysfunction the E/A ratio can show pseudonormal values but the e'/a' ratio remains pathological and thereby helps to discriminate between a normal filling pattern and pseudonormalization).[74,75]

With the VevoStrain Software a 2D-Strain analysis was performed of PSLAX B-Mode. By tracing the endocardium, Global Longitudinal Strain (GLS, [%]) and average radial displacement [mm] were calculated. Through Strain analysis the deformation of the left ventricular wall can be measured and provides additional information about the heart function. The GLS in healthy mice should be around -20%. The negative value means that the wall is shortening longitudinally in systole. If -e.g., due to an infarction- the shortening is impaired, the GLS will be higher and the |GLS| decreased. In the same analysis the radial displacement of different areas of the ventricular wall and their mean is calculated: average radial displacement. The possibility to look at the areas separately gives a deeper insight in where the left ventricular wall movement is impaired.[76]

3.1.5. Organ harvesting

To perform molecular biological analyzes with the hearts the mice were killed via perfusion. An incision of the abdomen under the rib cage was made and the left ventricle was punctured to remove a final blood sample (about 1ml). After

centrifugation in a heparin tube (MiniCollect® 0.8ml Lithium heparin gel, Interpath) the blood plasma was separated and stored at -80°C. The diaphragm of the animal was incised, and the circulation was rinsed via the left ventricle 2 minutes with heparin in NaCl 0.9% (50 IU/ml) through a 30G cannula while the inferior vena cava was opened to drain the blood from the circulation. The heart was removed, prepared (the right ventricle was separated, and the left ventricle was cut into three pieces), directly frozen in liquid nitrogen, and then stored at -80°C. The perfusion was performed by Simon Geißen and the subsequent blood and organ preparation were performed by me.

3.2 Molecular biological methods

3.2.1. Real time qPCR

(1) RNA-Isolation

The RNA was isolated using the miRNeasy Mini Kit by QIAGEN (cat. No. 217004) following the associated protocol.

(2) Reverse Transcription

The reverse transcription was performed with the QuantiTect® Reverse Transcription Kit (cat. No. 205311) following the associated protocol.

(3) Realtime PCR (using Taq®Man Assay)

The PCR reaction mix was prepared and transferred to the wells of a 96 well plate: 10µl TaqMan® Fast Advanced Master Mix (2x), 1µl TaqMan® Assay (GAPDH, 20x, PN4448490), 1µl TaqMan® Assay (CXCL2, 20x, PN4453320, FAM) and 6µl Nuclease-Free Water per well. 2µl of cDNA template and Nuclease-Free Water as a negative control were added to the wells. For each sample a double determination was performed. The reaction plate was sealed with optical adhesive film and centrifugated briefly. The PCR was performed in a QuantStudio™ 1 Real-Time-PCR-system according to the following protocol (Table 3.2):

UNG incubation	Polymerase activation	PCR (40/60 cycles)	
Hold 50°C	Hold 95°C	Denature 95°C	Anneal/ Extend 60°C
2 minutes	2 minutes	1 second	20 seconds

Table 3.2: Protocol for qPCR (Taq®Man Assay)

(4) Realtime PCR (using GoTaq® qPCR Master Mix)

The PCR reaction mix was prepared and transferred to the wells of a 96 well plate: 5µl GoTaq®qPCR Master Mix (2X), 1µl Forward Primer (20x), 1µl Reverse Primer

(20X, detailed list of primers see table 3.1), 0,1µl CXR Reference Dye and 0,9µl Nuclease-Free Water. 2µl (10ng) of cDNA template and Nuclease-Free Water as a negative control were added to the wells, again in double determinations. The reaction plate was sealed with optical adhesive film and centrifugated briefly. The PCR was performed in a QuantStudio™ 1 Real-Time-PCR-system according to the following protocol (Table 3.3):

Polymerase activation	PCR (40 cycles)	
Hold 95°C	Denature 95°C	Anneal/ Extend 60°C
2 minutes	3 seconds	30 seconds

Table 3.3: Protocol for qPCR (GoTaq® qPCR Master Mix)

Gene of interest	Sequence forward primer	Sequence reverse primer
GAPDH	5'-TCC CAC TCT TCC ACC TTC-3'	5'-CTG TAG CCG TAT TCA TTG TC-3'
BNP	5'-AGA CCC AGG CAG AGT CAG AA-3'	5'-CAG CTC TTG AAG GAC CAA GG-3'
Col1a1	5'-CGA CCT CAA GAT GTG CCA CT-3'	5'-ACT CGA ACG GGA ATC CAT CG-3'
Col3a1	5'-GCC TTC TAC ACC TGC TCC TG-3'	5'-TTC CTC CCA CTC CAG ACT TG-3'
PAI-1	5'-CAC AGG CAC TGC AAA AGG TC-3'	5'-GGA TTG TCT CTG TCG GGT TGT-3'
ERK1	5'-ACA CTG GCT TTC TGA CGG AG-3'	5'-TGA TGC GCT TGT TTG GGT TG-3'
ERK2	5'-GCA AGG GAG AGA TGG TGT AAG-3'	5' ACCGAC ATC TGA ACT CGT CC-3'
Tgfβ	5'-TGG TCC AGT CTG CTT CGT CT-3'	5'-CAC AAG AGC AGT GAG CGC TGA A-3'
Tgfβ Receptor 1	5'-TGG TCC AGT CTG CTT CGT CT-3'	5'GTG GTG CCC TCT GAA ATG AA-3'

Table 3.4: Primers used for qPCR; Gapdh was used as a housekeeping gene.

3.2.2. SDS-Page and Western Blot

(1) Protein isolation

The sample lysis was performed in the lysis buffer RIPA (Radio Immuno Precipitation Assay, recipe see appendix) mixed with Phosphatase Inhibitor (PhosSTOP EASYpack, Roche) and Protease Inhibitor (cOmplete Tablets Mini EDTA-free EASYpack, Roche). 300µl of this buffer were placed together with the sample into a Precellys Lysing Kit (P000918-LYSK0-A) and were mechanically lysed 3 times for 20 s in a Precellys® 24 tissue homogenizer (Bertin instruments). After incubating 30 minutes on ice the sample was centrifuged for 30 minutes at 14000 rcf and 4°C.The supernatant was transferred into a new tube. To determine the concentration an BCA-Assay was performed with a part of the sample.

(2) BCA-Assay

In a 96-well plate 10µl sample/well were pipetted and 200µl reagent/well were added (reagent: Pierce™ BCA Protein Assay Kit, ThermoScientific™). After an incubation of 30 minutes at 37°C the samples were measured in the photometer and concentrations were calculated in comparison to a dilution series.

(3) SDS-PAGE

After diluting the samples to the same concentration, 4x Laemmli Sample Buffer (recipe see appendix) was added (3:1) to each sample. For the SDS-PAGE 40µl sample and 20µl molecular weight marker (Thermo Scientific™ PageRuler™ Plus Prestained Protein ladder, 10 to 250kDa) were pipetted into the wells of a Mini-Protean® TGX™ Precast-Gel (15well comb, 15µl/well). After a setting time of 30 minutes the gel electrophoresis was started at 70V and after 10 minutes continued with 100V (Recipe Running Buffer see appendix).

(4) Western Blot

The gel was blotted to a Rotilabo® Blotting paper (thickness: 1.5mm) in a Trans-Blot® Turbo™ Transfer System (BIO-RAD) for 30 minutes at 2.5 A and 10V (Recipe Transfer Buffer see Appendix). A Ponceau coloration was made to control correct transfer of proteins. Then the membrane was incubated 30 minutes in the blocking solution and then incubated with a primary antibody (details see Table 3.5). A washing step with TBS/T (3 times 10 minutes) was performed before incubation 2 hours with a secondary antibody labeled with peroxidase. Another washing step was made before measuring the fluorescence in a Fusion FX Vilber Lourmat (Peqlab) with Amersham™ ECL™ Western Blotting Detection Reagents (GE Healthcare) or SuperSignal™ West Femto Maximum Senstitivity Substrate (Thermoscientific).

Protein of interest	Molecular weight (kDa)	Block-ing solution	Primary Antibody (dilution)	Incubation Time	Secondary antibody (dilution)	Host
GAPDH	146kDa (detected on membrane: fragment of 37kDa)	BSA (3% in TBS)	Cell signaling 2118L Host: rabbit (1:7500)	2 hours	Anti-rabbit Peroxidase, Vector PI-1000 (1:10000)	Goat
Phospho-p44/42 MAPK (ERK1/2)	42/44kDa	BSA (5% in TBS)	Cell signaling 9101 Host: rabbit (1:1000)	Overnight	Anti-rabbit Peroxidase, Vector PI-1000 (1:10000)	Goat
p44/42 MAPK (ERK1/2)	42/44kDa	BSA (5% in TBS)	Cell signaling 4695 Host: rabbit (1:1000)	Overnight	Anti-rabbit Peroxidase, Vector PI-1000 (1:10000)	Goat

Table 3.5: Antibodies used for Western Blots; GAPDH was used as housekeeping gene.

3.3 Histological methods

All the images were taken in a Keyence All-in-one Fluorescence Microscope (BZ-X800) if not explained otherwise.

3.3.1. Cryosections

After harvesting the hearts were embedded in OCT Compound (Optimal cutting temperature Compound) and cut with a cryotome in 8µm sections. They were stored in a -80°C freezer until further processing.

(1) H&E-Staining

The slides were fixed for 10 minutes in Acetone and after drying stained in Hem alum solution acid acc. To Mayer (ROTH, Art.-Nr. T865.2) for 1.5 minutes. They were rinsed shortly with Aq. dest. and then blued for 10 minutes in running tap water. After staining for 1 minute in Eosin Y solution 0.5% in water (ROTH, Art.-Nr.

X883.2) they were dipped shortly in 96% Ethanol twice and then immersed for 1 minute in Roti®Histol (ROTH, Art.-Nr. 6640.4) and mounted with Eukitt® Quick-hardening mounting medium.

To evaluate the trophic of the hearts 30 images were acquired from each sample in a 40-fold magnification. In each image the cross-sectional area of 10 cardiomyocytes was determined using the analyses software BZ-X800_Analyzer © 2018 Keyence Corporation.

The means of the cross-sectional area of the 300 cells/sample were compared to each other.

(2) Picrosirius Red Staining

The slides were dipped for 1 minute each into a descending alcohol series (100%, 96%, 70% ethanol). They were stained 2.5 minutes in Weigerts Eisenhämatoxylin (solution Ferri-Hematoxylin A and B 1:1) and then blued 10 minutes in running tap water. After rinsing shortly in Aq. dest the were dipped into 1% HCl in 96% ethanol. They were stained in Picrosirius Red for 3 minutes and differentiated again shortly in 1% HCl. After this they were dipped for 1 minute each into an ascending alcohol series (70%, 96%, 100% ethanol) and immersed twice for 1 minute in Roti®Histol (ROTH, Art.-Nr. 6640.4) and mounted with Eukitt® Quick-hardening mounting medium.

To investigate fibrosis, 20 images were acquired from each sample in a 20-fold magnification. In each image the percentage of fibrosis was analyzed using the Hybrid cell-count tool of BZ-X800_Analyzer © 2018 Keyence Corporation.

3.3.2. Paraffin sections

As the hearts used for the cryosections had been injected with siRNA prior to harvest and heart morphology is better conserved in paraffin sections than in cryosections I repeated the histology on parrafin sections of mice that were not injected with siRNA to get more valid results.

The harvest of the total hearts for the paraffin sections was performed under the hood with mice in an injection narcosis. The mouses circulation was first rinsed 2 minutes with 5 mL heparin in PBS (50 IU/ml) and then for 2 minutes with 5mL 4% methanol-free formaldehyde in PBS. The hearts were removed and fixated overnight in 0.5mL 4% methanol-free formaldehyde in PBS. The next day they were stored in PBS until embedding. After embedding in paraffin, the hearts were cut with a microtome into 4µm slices and stored at room temperature until further processing.

Before each staining the slides were deparaffinized according to the same protocol: 2 x 5 min RotiHistol® and then 5 min each in a descending ethanol concentration (100%, 95%, 70%, Aq. dest).

(1) H&E-Staining

The slides were stained in Hem alum solution acid acc. To Mayer (ROTH, Art.-Nr. T865.2) for 5 minutes. They were rinsed shortly with Aq. dest. and then blued for 10 minutes in running tap water. After staining for 2 minutes in Eosin Y solution 0.5% in water (ROTH, Art.-Nr. X883.2) the slides were passed through an ascending alcohol concentration (Aq. dest, 70%, 95%, 100%; 5 minutes each) and immersed in RotiHistol® for 2 minutes before mounting with Eukitt® Quick-hardening mounting medium. The pictures were taken with a SlideScanner (Hamamatsu S360) and then analyzed in QuPath. For each sample the cross-sectional area of 100 myocytes was determined and the means were compared to each other.

(2) Picrosirius-Red Staining

The Picrosirius-Red Staining was performed with a Connective Tissue Stain Kit (ab150681) according to the associated protocol. The pictures were taken with a SlideScanner (Hamamatsu S360) and then analyzed via using the pixel classification tool in QuPath. A pixel classifier was trained on 3 different examples in which manually fibrotic areas (stained yellow) and non-fibrotic heart tissue (stained red) were identified. This pixel classifier was then used to determine in each sample the percentage of fibrosis.

3.4 Single-cell RNA sequencing

Fluorescence-activated cell sorting (FACS) is a certain type of flow cytometry in which -as the name indicates- the cells are sorted additionally to the regular process of flow cytometry. In our experiments the cells were sorted in a BD FACSAria IIIu. to perform subsequent single-cell RNA sequencing.

The principle of FACS is the following: Cells out of a sample are directed in a laminar stream one by one past a laser. The passing of a cell leads to redirection of the monochromatic light emitted by the laser and the detection of these signals allows to characterize the cell. The Forwardscatter (FSC) gives information about the size of a cell and the Sidescatter (SSC) about the granularity. Additionally, the cells are stained before the process with specific fluorescent antibodies and measuring this fluorescence provides more detailed information about the cell. The choice of fluorophores is crucial for the experiment as similar emission wavelengths complicate the assignment of a signal to a specific antibody (see Table 3.6 for further information on the fluorophores

used in the experiments). This is also the reason why bead controls are needed. They contain species specific antibodies and are stained simultaneously to the samples with only one fluorescent antibody each. Before measuring the samples each of the bead controls is measured separately. Because they are only stained with one fluorophore the negative and positive population can be distinguished and false positive signals in channels meant for another fluorophore can be compensated by adjusting thresholds. To sort the cells after the flow cytometry, the laminar flow is broken after passing the laser into droplets containing each one cell. These droplets are then given either a positive, a negative or no charge dependent on the signal that was detected during flow cytometry. Thereby, only a certain cell type - defined by cell size, granularity and specific antibody binding properties - is guided into collection tubes and available for further analyses. [77]

Fluorophore	Excitation Peak [nm]	Emission Peak [nm]
FITC	494	518
PE	496, 566	576
PE-Cyanin7	570	780
Brilliant Violet 711	410	715
AlexaFluor® 647	653	669
APC/Cyanine7	650, 755	660, 775

Table 3.6: Excitation Peak and Emission Peak wavelengths for fluorophores used in this thesis (Source: manufacturer information)

3.4.1. Organ harvest and sample preparation

After taking a blood sample out of the left ventricle (about 1ml) the mouses circulation was rinsed with 20mL PBS. One part of the blood was collected in an EDTA tube and analyzed with the veterinary hematology analyzer (Element HT5 by Heska). The rest of the blood was centrifuged in a heparin tube (MiniCollect® 0.8ml Lithium heparin gel, Interpath) and the plasma then stored at -80°C for further analyses.

The heart was harvested, and the atria were removed before the heart was weighed and stored in 2mL of PBS in a 24 well plate.

When all samples were collected, they were placed each in 1mL of digestion buffer:

Ingredient	Concentration	Volume per sample [µl]
Collagenase I	450 U/ml	45
Collagenase XI	125 U/ml	10
Hyaluronidase	60 U/ml	5
DNAse	60 U/ml	3.7
HEPES buffer	1X	20
PBS	1X	916.3
Total		1000

Table 3.7: Recipe for FACS digestion buffer

In this buffer the hearts were first minced with scissors, vortexed quickly and then incubated for 1h at 37°C in a shaker at 350 rpm. The cell suspension was then meshed through a 70µm mesh into a 50ml falcon. The falcons were centrifuged for 7 minutes at 4°C at 350 rpm and decanted. The pellet was resuspended in 300µl FACS buffer (0.5% BSA/PBS), vortexed and then filtered again through a 35µm mesh into a FACS tube. After a short centrifugation of the FACS tube with the purpose of drying the mesh, 10µl of each sample were diluted with 180µl of PBS for cell counting. Of one sample 50µl were taken as an unstained sample in a separated FACS tube. The samples were then stained for 20 minutes with 50µl of the master mix containing 0.5µl of each antibody (Table 3.8).
Also bead controls were prepared: for each of the six fluorophores used in the panel (Table 3.7) 0.5µl of an antibody labeled with the fluorophore was added to one drop of OneComp eBeads (REF#: 01-111-42, Invitrogen) in a FACS tube.

Target	Fluorophore	Cat#; Company
Ly-6C	FITC	553104; BD Biosciences
TER-119/ Erythroid Cells	PE	116208; BioLegend
NK-1.1	PE	108708; BioLegend
CD90.2	PE	553008; BD Biosciences
Ly-6G	PE	551461; BD Biosciences
CD45R/B220	PE	553089; BD Biosciences
F4/80	PE-Cyanine7	123113; BioLegend
CD45	Brilliant Violet 711	103147; BioLegend
CD64	Alexa Fluor® 647	558539; BD Biosciences
CD11b	APC/Cyanine7	101226; BioLegend

Table 3.8: List of fluorescence labeled antibodies used for flow cytometry.

After staining the cells were washed: 4.5mL of FACS buffer were added to the sample and the tubes were centrifuged again for 7 minutes at 4°C at 350 rpm. The tubes were decanted, and the washing was repeated once. The pellet was resuspended in 300µl FACS buffer and the tubes placed on ice. Right before sorting the samples in a BD FACSAria IIIu. they were filtered again through a 35µm filter.

3.4.2. Single-cell RNA sequencing

The cells were sorted for CD45-positive cells, a receptor protein tyrosine phosphatase specific for leukocytes, and stained with DAPI for quality control.[78,79]
The cells of this CD45-positive single cell suspension were then isolated, and an individual reaction mixture was added that contained a unique barcode for each cell and sample. The following reverse transcription resulted in cDNA in which this barcode was integrated and thereby marked every single cell. This cDNA was then mixed, amplified via PCR, and sequenced.[80] The single-cell RNA sequencing process starting with cell quality control and cell isolation was performed by the Cologne Center for Genomics.
The following bioinformatic analysis of the data was performed by Simon Geißen: A filtered feature matrix generated by the Cell Ranger pipeline was clustered using the leiden algorithm. Cell clusters whose enrichment profile matched with previously reported expression patterns of macrophages were reclustered, again using the leiden algorithm. Within the resulting 16 clusters of macrophages, we performed differential gene expression analysis and subsequently performed enrichment analyses using the gene ontology and hallmark databases. Bioinformatic processing was performed by the python framework scanpy.[81]
Different methods were used for the visualization of the single cell data: Uniform Manifold Approximation and Projection (UMAP), Heatmaps and Volcano Plots. The enrichment analysis was performed with the Gene Ontology (GO) database.

3.5 Statistical analyses

All statistical analyses were performed with GraphPad Prism. The level of significance chosen was always α=0.05.

3.5.1. T-test

The standard formula of the t-test is:

$$t = \frac{Mean1 - Mean2}{Standard\ Error\ of\ the\ Mean}$$

A t-test is used to compare a rather small number of samples (under 30) to a mean or between different groups. There are some preconditions that need to be fulfilled for using a t-test: comparison of only one variable, numeric data, a maximum of two groups, a random sample, and normally distributed data. That's why all the data on which a t-test was performed were previously tested on Gaussian distribution. For this purpose, a D'Agostino&Pearson test was performed. If the number of samples was too small (<8) to perform this test, a Shapiro-Wilk test was performed. If the data was not normally distributed a Mann-Whitney test was performed instead of t-test.

All t-tests performed in this thesis were performed on unrelated data, so an unpaired samples t-test was used. As the hypothesis in the experiments was always: "Is there a difference between the groups?" without specifying the direction of the potential difference a two-tailed t-test was used. To perform a normal unpaired samples t-test the two sets of data need to have identical variances. This assumption was tested using an F test and the analysis was only performed if the variances were not significantly different ($p<0.05$). Otherwise, a Welch's t-test was performed.[82]

3.5.2. ANOVA

ANOVA is short for Analysis of variance and is used to compare the means of three or more groups to each other. Similar as in t-test the data has to be numeric, a random sample selection is needed, and the data should be normally distributed which is why the tests for Gaussian distribution were made accordingly to the explanation for t-test. When data was not normally distributed a Kruskal-Wallis test was performed (only for One-Way ANOVA). The variance between the groups was also tested using Bartlett's test to differ not significantly, as this is an assumption for ANOVA. If the n was too small to perform Bartlett's test, Brown-Forsythe test was performed. If it differed significantly, a Welch's ANOVA test was performed (only for One-Way ANOVA). As a follow-up of the ANOVA tests a multiple comparison test was performed to compare the mean of each column to the mean of every other column via Tukey's multiple comparison test. The Kruskal-Wallis test was combined with a Dunn's multiple comparison test, the Welch's ANOVA with a Dunnett's T3 multiple comparison test. There are different forms of ANOVA depending on the experimental design.

When a single factor was measured in three or more different groups, then a One-way ANOVA was performed.

When two different factors were concerned in an experiment a Two-Way ANOVA was performed. For a Two-Way ANOVA the assumption of Gaussian distribution

is not too important with large sample sizes so sometimes it was performed although not all samples were normally distributed. If so, it is mentioned in the Results section.[83]

When data was obtained from the same subject group at different timepoints a repeated measures ANOVA was performed, in this thesis always One-way because there was always only one factor concerned. Sometimes this analysis was not possible because data did not exist for every subject at every timepoint. In this case the data was compared using a mixed-effect analysis. For nonparametric data a Friedman test should be performed instead of a repeated measures ANOVA. As this test cannot be performed with missing values, a Kruskal-Wallis test was performed instead.[84]

4. Results

The objective of this thesis was to determine the chronic effects that CLP has on mice with a special focus on the heart. Therefore, the immune response was observed via weekly blood samples, the heart function via echocardiography, the acute effects on the heart via qPCR and Western Blot 1 week after CLP and the chronic effects on the heart via qPCR, single-cell RNA sequencing and histological methods, such as H&E staining and Picrosirius-Red Staining, 7 weeks after CLP (Figure 4.1).

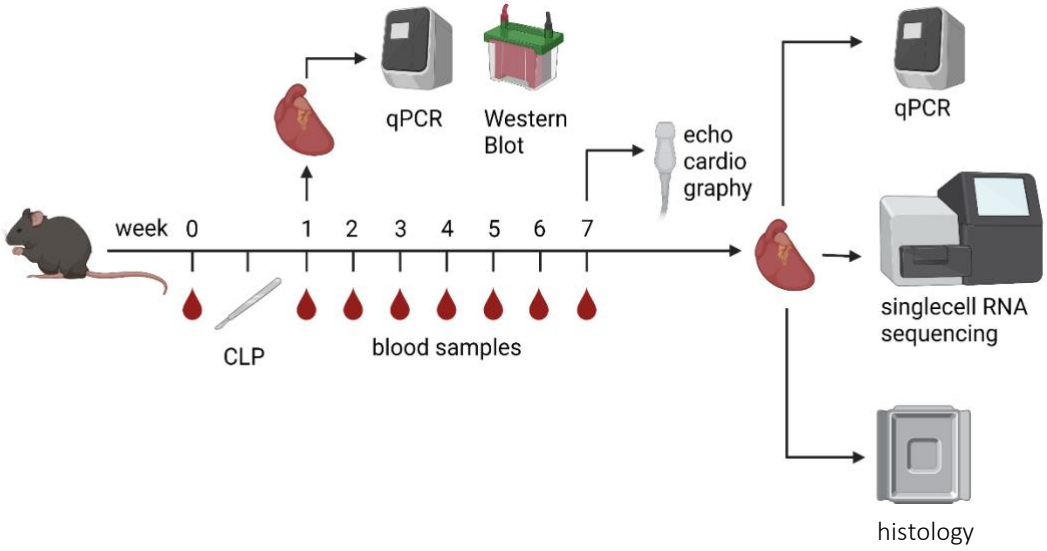

Figure 4.1: Experimental design

4.1 Immune response after CLP

CLP leads to an increased white blood cell count compared to baseline for 6 weeks (Figure 4.2, A). This increase is mainly driven by neutrophils, which increase in number and percentage of total white blood cells similarly (Figure 4.2, B-C). Lymphocytes however do not increase in number and therefore decrease in percentage of total white blood cells (Figure 4.2, D-E). Monocytes, eosinophils and basophils count increases in response to CLP, too, but due to their low absolute numbers do not influence total white blood cell count relevantly (Figure 4.2, F-H).

The CLP surgeries and subsequent experiments were performed on male and female mice. In order to rule out differences in the results due to sex, the blood immune cell reaction in male and female mice was analyzed. At baseline male and female mice show a significantly different immune cell distribution: male have a higher neutrophil percentage and accordingly a lower lymphocyte percentage of

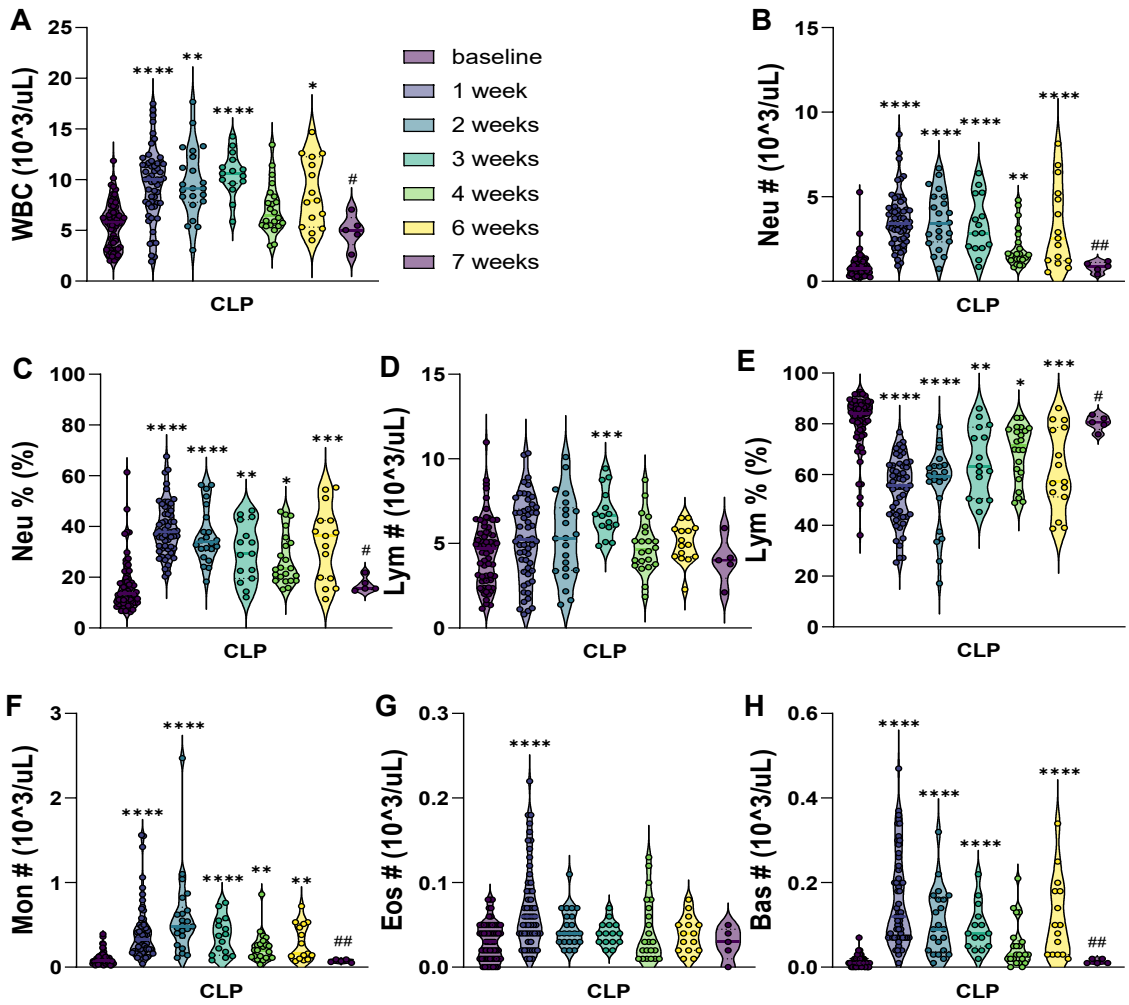

Figure 4.2: CLP induces neutrophilia for about 6 weeks.
Leukocytes in weekly blood work after CLP. A) Total White Blood Cell Count. Absolute (B, D, F, G, H) and relative (C, E) distribution of white blood cell subtypes (neutrophils, lymphocytes, monocytes, eosinophils, basophils).
Mixed-effect analysis + Tukey‘s multiple comparison (A, D); Kruskal-Wallis + Dunn‘s multiple comparison (B, C, E-H): In comparison to baseline: * = p<0.05, ** = p<0.01,
*** = p<0.001, **** = p<0.0001; In comparison to 1 week: # = p<0.05, ## = p<0.01.

white blood cells (Figure 4.3, C, E). Also, the standard deviatiation (SD) of neutrophil absolute count and percentage are higher in male: SD (Neu # [10^3/µL]) = 1.038 (male) and 0.255 (female); SD (Neu % [%]) = 12.49 (male) and 2.879 (female); F test to compare variances shows significant difference: p<0.0001 in both. However, both sexes react similarly to CLP surgery. One week after CLP both show a leukocytosis mainly driven bei neutrophilia and there is no significant difference between means in neutrophil count or percentage (Figure 4.3). In both sexes the standard deviation of neutrophil absolute count increases: SD (Neu # [10^3/µL]) = 1. 749 (male) and 1.434 (female); F test to compare variances shows no significant difference: p=0.34. The standard deviation of neutrophils percentage decreases in male and increases in female but F test shows no siginificant difference in variance 1 week after CLP: SD (Neu % [%]) = 8.734 (male) and 11.92 (female); F test: p= 0.15.

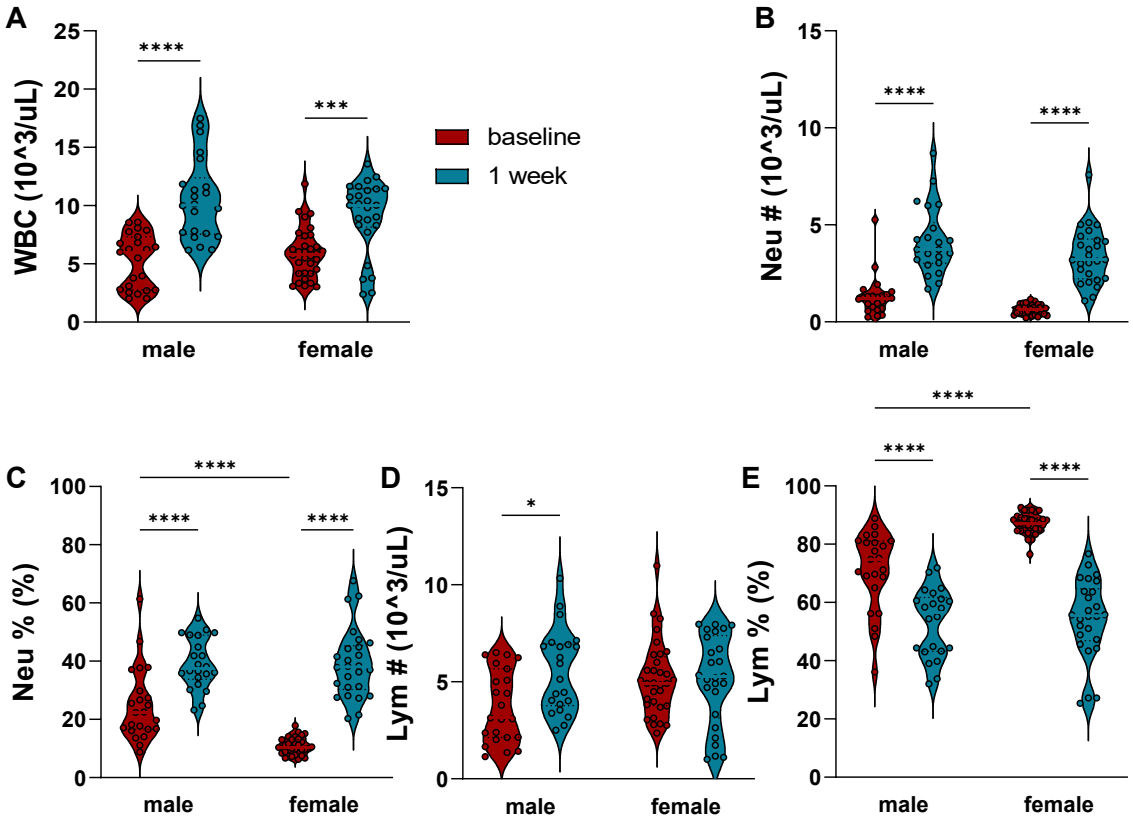

Figure 4.3: The immune reaction to CLP is similar in female and male mice despite baseline differences.
White Blood Cells after CLP in male and female mice. A) Total White Blood Cell Count. Absolute (B, D) and relative (C, E) distribution of white blood cell subtypes (neutrophils, lymphocytes)
Two-way ANOVA + Tukey's multiple comparison: * = $p<0.05$, ** = $p<0.01$, *** = $p<0.001$, **** = $p<0.0001$ (Because of high n (>22 in all samples) Two-Way ANOVA was performed despite not all samples are normally distributed (A-D) and the Standard deviation differs between samples significantly in B, C and E (Barlett's test: $p<0.0001$)

4.2 Heart function after CLP

To determine whether cardiac function is chronically impaired by CLP surgery, echocardiographic analyses were performed 7 weeks after surgery. Systolic function was analyzed via ejection fraction (EF [%]), cardiac output [ml/min], global longitudinal strain (GLS, [%]), and radial displacement [mm]. Neither parameter shows differences between control and CLP (Figure 4.4, A-D). Brain natriuretic peptide (BNP) is a parameter used for diagnosis of heart failure. The expression of BNP is increased - though not significantly ($p=0.0529$) – 7 days after CLP compared to control (Figure 4.4, F). 8 weeks after CLP however, there is no difference in BNP-expression between sham and CLP animals ($p=0.4191$; Figure 4.4, G).

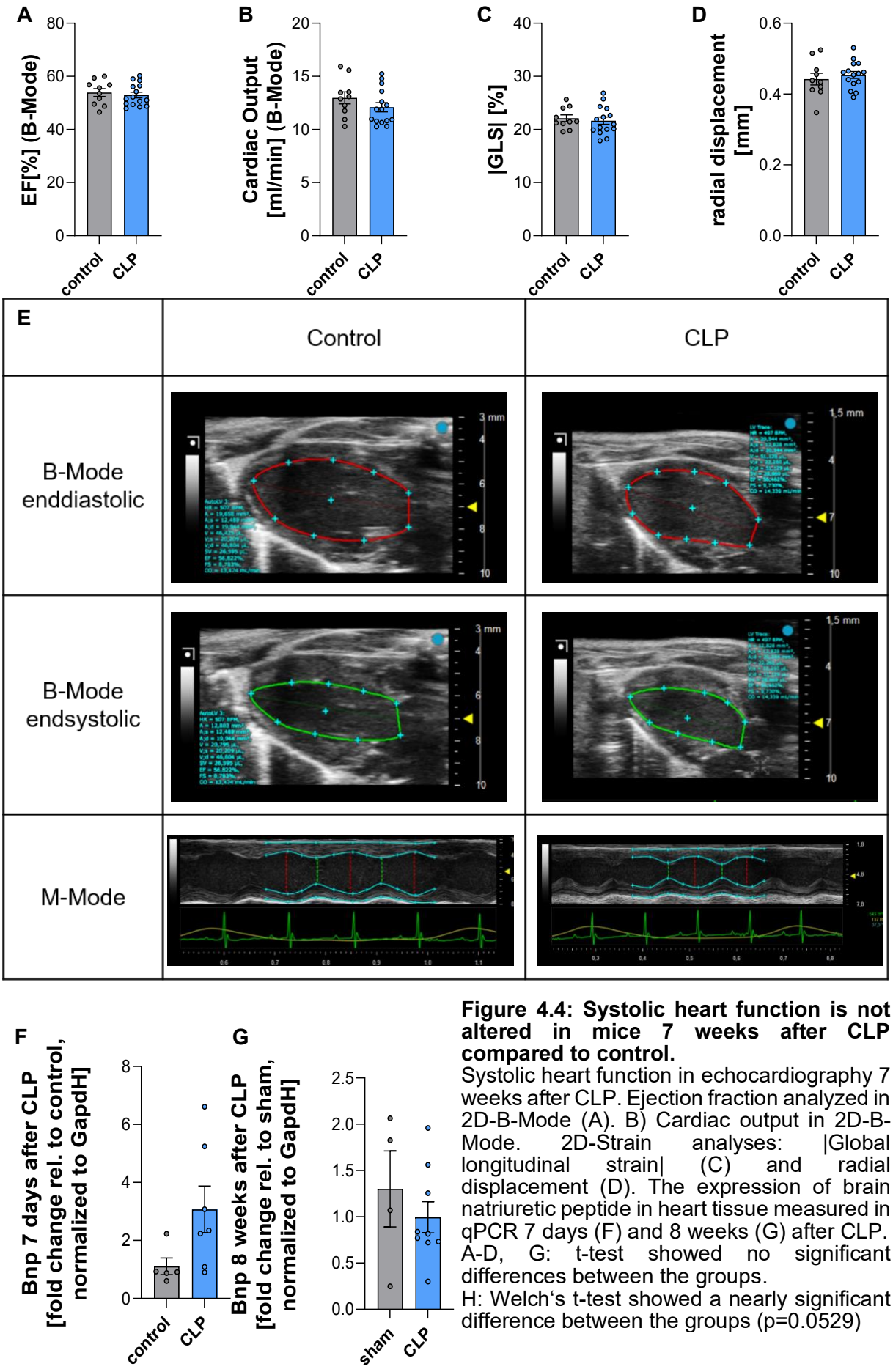

Figure 4.4: Systolic heart function is not altered in mice 7 weeks after CLP compared to control.
Systolic heart function in echocardiography 7 weeks after CLP. Ejection fraction analyzed in 2D-B-Mode (A). B) Cardiac output in 2D-B-Mode. 2D-Strain analyses: |Global longitudinal strain| (C) and radial displacement (D). The expression of brain natriuretic peptide in heart tissue measured in qPCR 7 days (F) and 8 weeks (G) after CLP. A-D, G: t-test showed no significant differences between the groups.
H: Welch's t-test showed a nearly significant difference between the groups (p=0.0529)

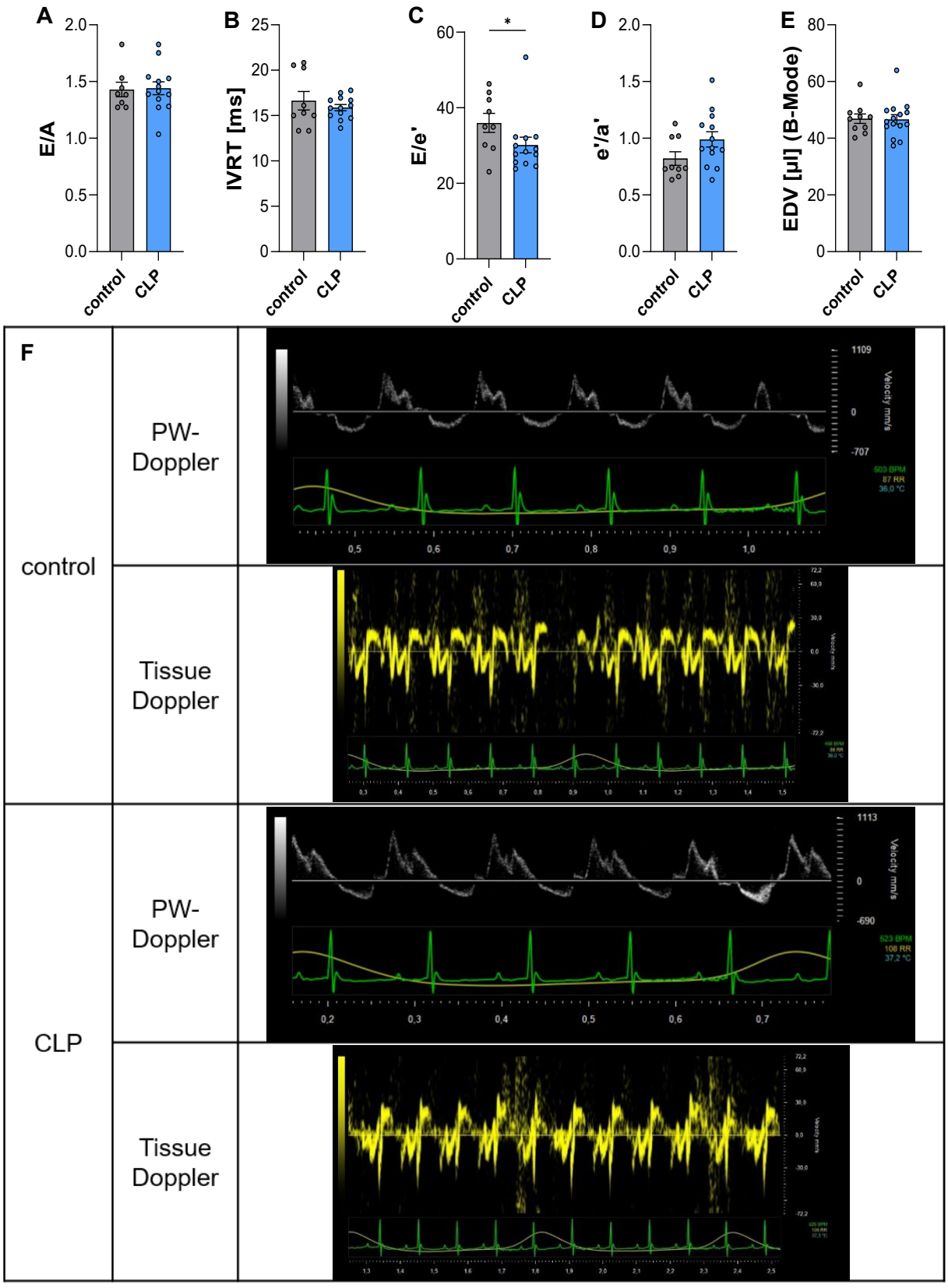

Figure 4.5: Diastolic heart function is not worsened in mice 7 weeks after CLP compared to control.
Diastolic heart function in echocardiography 7 weeks after CLP. A) E/A, B) Isovolumetric relaxation time, C) E/e‘ as equivalent to left ventricular end-diastolic pressure, D) e‘/a‘, E) End diastolic left ventricular volume.
A, B, D, E: no significant difference in Mann-Whitney (A, E), Welch‘s t-test (B) and t-test (D), C: Mann-Whitney test, * = $p<0.05$

Diastolic heart function was analyzed via E/A, isovolumetric relaxation time (IVRT [ms]), E/e', e'/a' and end diastolic left ventricular volume (EDV [µl]). E/A, IVRT, e'/a' and EDV show no significant difference between control and CLP. E/e', a parameter in which a high value indicates diastolic heart dysfunction, is significantly lower in CLP mice (Figure 4.5).

4.3 Heart morphology after CLP

H&E staining was performed on cryosections to analyze myocyte cross-section and detect possible cardiac hypertrophy. The cardiomyocyte cross-section does not differ significantly between sham and CLP animals 8 weeks after CLP (Figure 4.6, A). As tissue sections lacked in quality due to tissue tears, the staining was repeated on paraffine sections which show better results for tissue integrity (Figure 4.6, B). However, the cardiomyocyte cross-section 7 weeks after CLP compared to control does not differ either (Figure 4.6, B).

End diastolic left ventricular posterior wall thickness (LVPWd [mm]) is a parameter assessed by echocardiography that also represents hypertrophy and shows no difference between animals 7 weeks after CLP and control (Figure 4.6, C). Also, the heart weight [mg] between these two groups does not differ (Figure 4.6, D).

Picrosirius Red staining stains fibrotic tissue red and was therefore used to detect cardiac fibrosis. On cryosections there is no significant difference between animals 8 weeks after CLP and sham but a tendency to a higher percentage of fibrosis in CLP animals (Figure 4.7, A). However, this trend was not validated in the paraffine sections, where in control and CLP groups the percentage of fibrosis does not differ and shows a physiological level of 2-4% (Figure 4.7, B).

The expression of Collagen type 3α1 is significantly increased in CLP animals 8 weeks after surgery compared to sham (Figure 4.7, C). However, 7 days after CLP neither the expression of Collagen type 3α1 nor Collagen type 1α1 differs compared to control (Figure 4.7, D, E).

To further analyze if CLP leads to the activation of fibrosis inducing pathways, qPCR and Western Blot of heart tissue were performed 7 days after CLP. PAI-1 is protective for cardiac fibrosis.[85] Its expression is not altered compared to control (Figure 4.8, A). ERK1, ERK2, TGF-β nor TGF-β-Receptor 1 are fibrosis inducing proteins and the expression of neither of them is altered compared to control (Figure 4.8, B-E).[86] The phosphorylated form of ERK (pERK) is the active form of the fibrosis inducing protein, so the proportion between pERK and ERK represents the activity of the protein. This was analyzed via Western Blot and no significant difference was

found between control and 7 days after CLP (Figure 4.8, F, G; Supplementary Figure 7.4.1).

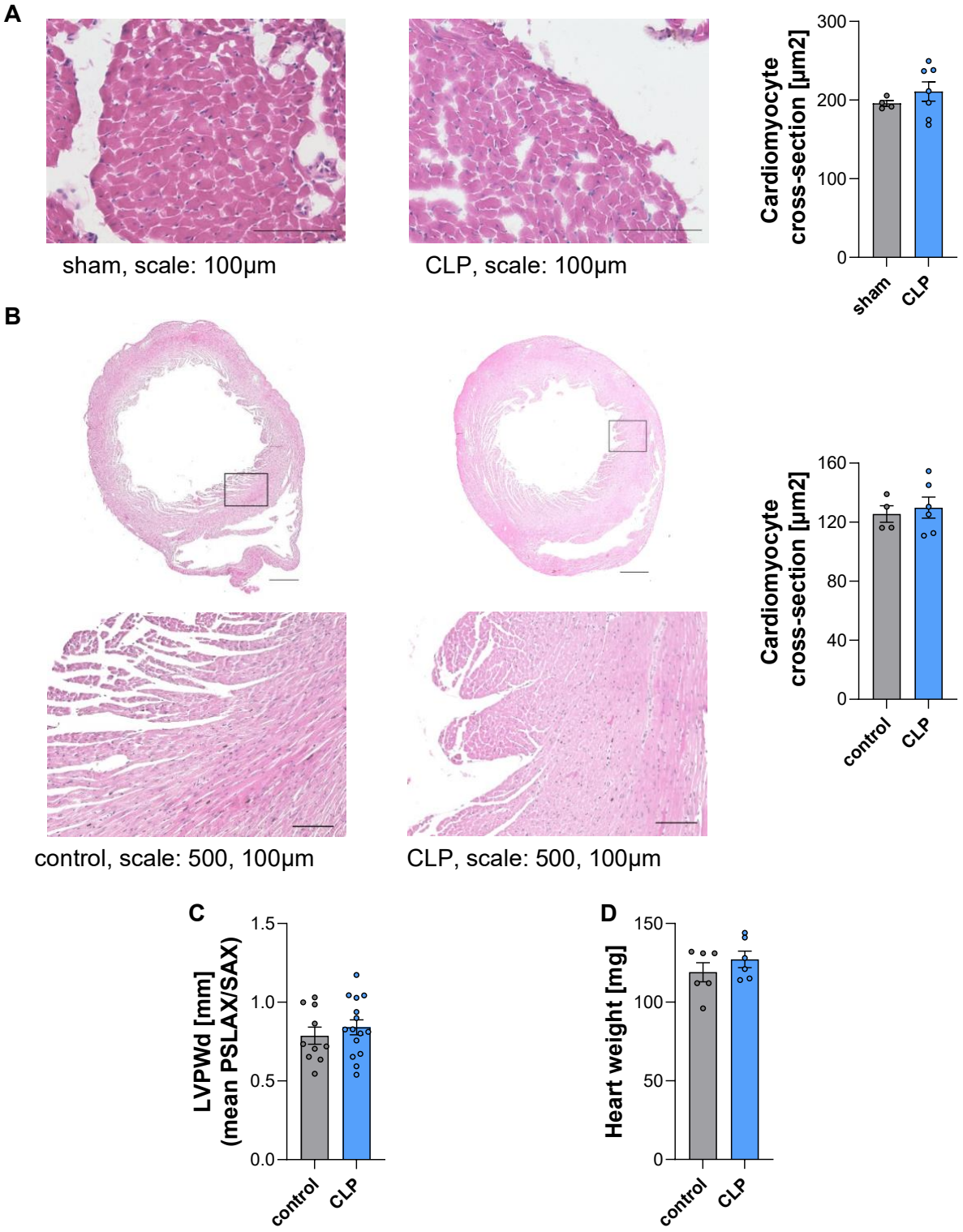

Figure 4.6: CLP does not lead to cardiac hypertrophy.
Cardiomyocyte cross-section analyzed in H&E-staining of cryo sections 8 weeks after CLP compared to sham (A) and paraffin sections 7 weeks after CLP compared to control (B). C) Left ventricular posterior wall thickness enddiastolic 7 weeks after CLP compared to control. D) Heart weight 7 weeks after CLP compared to control.
A: no significant difference in Welch‘s t-test
B-D: no significant difference in t-test

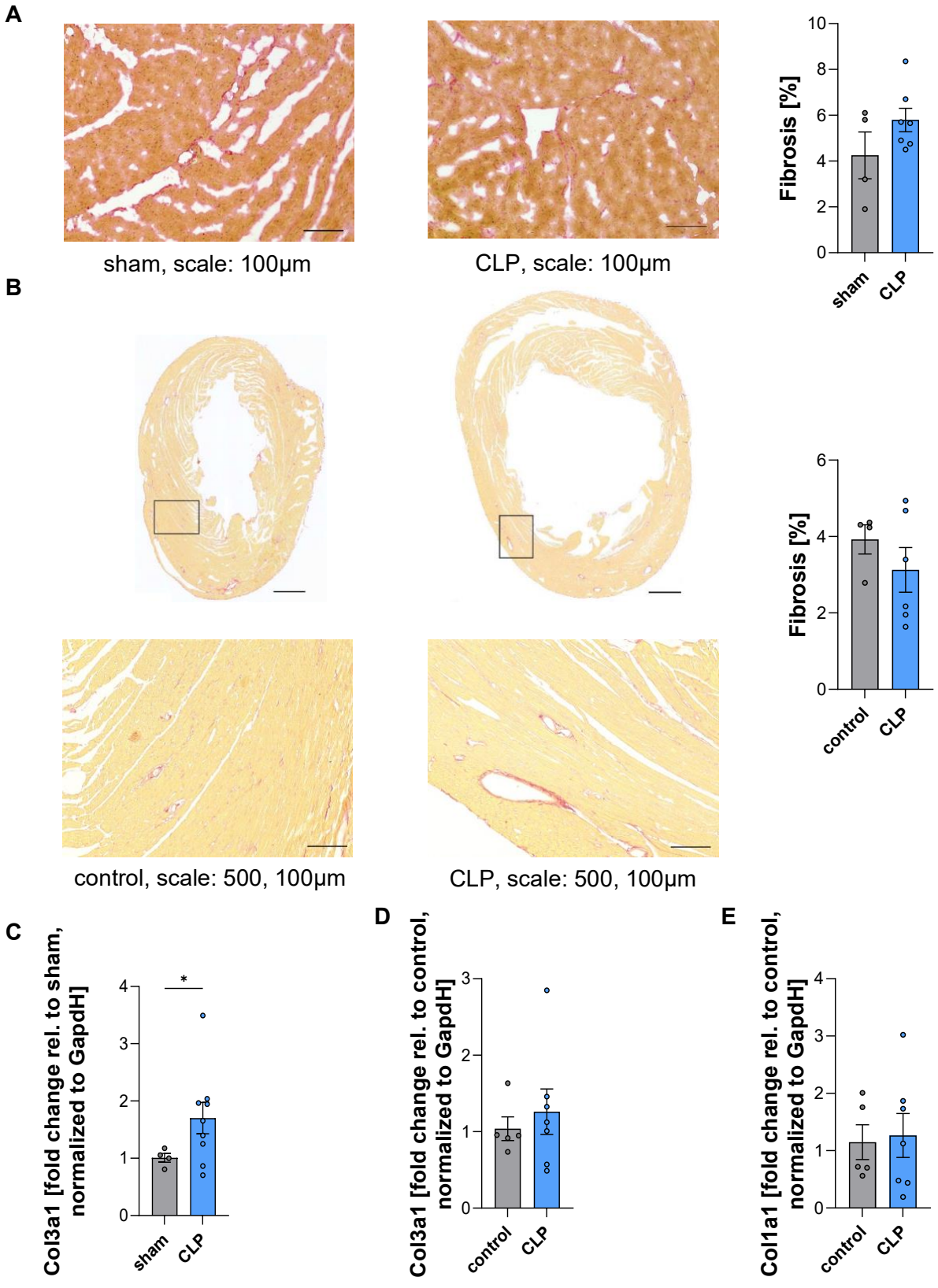

Figure 4.7: CLP does not lead to fibrotic changes in the myocardium.
Percentage of fibrosis in Picrosirius Red staining of cryo sections 8 weeks after CLP compared to sham (A) and paraffin sections 7 weeks after CLP compared to control (B).
Gene expression in heart tissue via qPCR of Collagen type 3α1 8 weeks after CLP compared to sham (C) and 7 days after CLP compared to control (D). E) Gene expression in heart tissue via qPCR of Collagen type 1α1 7 days after CLP compared to control.
A, B, D, E: no significant difference in t-test
C: Welch‘s test (* = $p<0.05$)

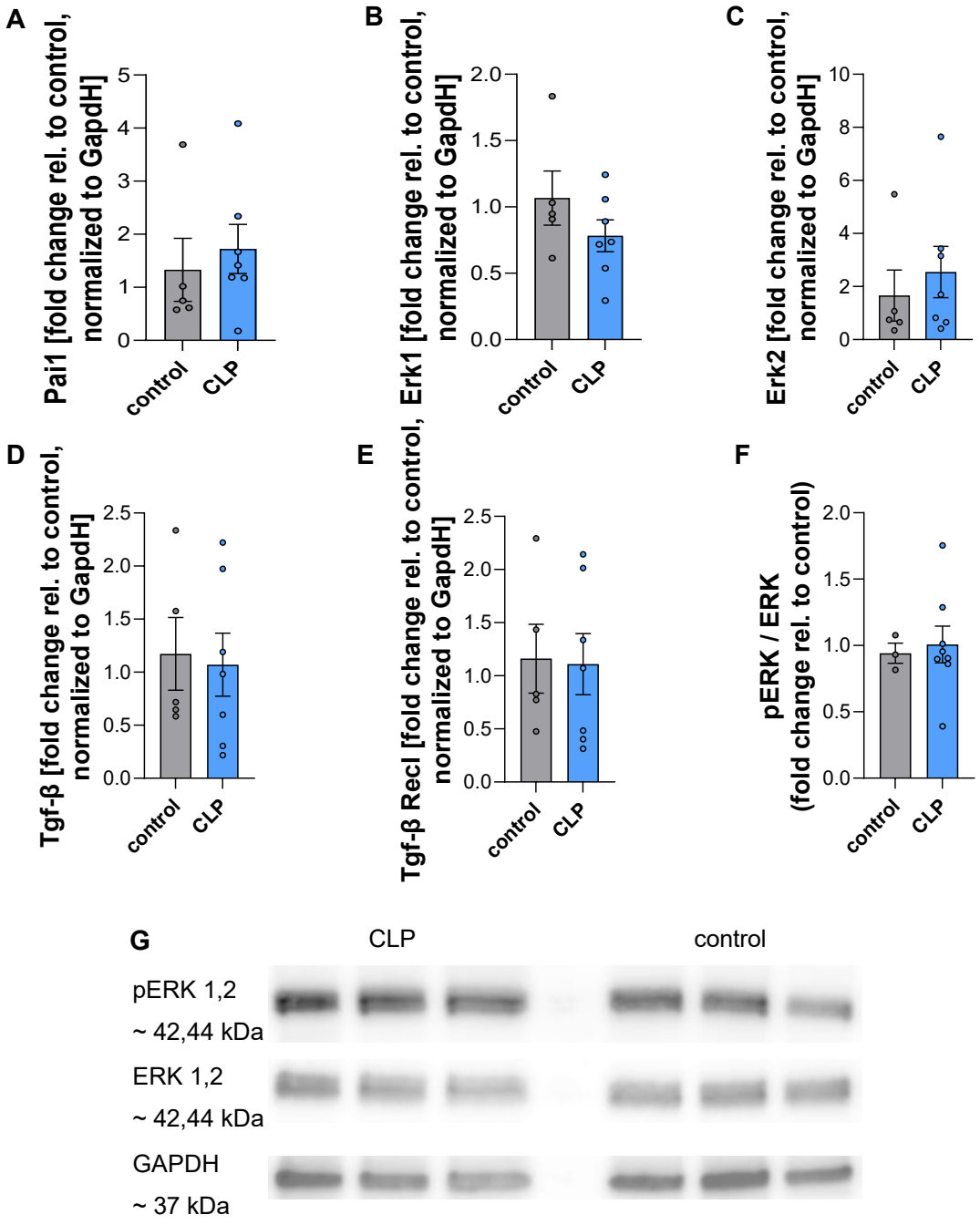

Figure 4.8: Fibrosis inducing pathways are not altered 7 days after CLP.
Gene expression in heart tissue via qPCR of A) Plasminogen activator inhibitor-1, B) Extracellular signal-regulated kinase 1, C) Extracellular signal-regulated kinase 2, D) Transforming growth factor β and E) Transforming growth factor β-receptor I. F, G) Protein expression in heart tissue via Western Blot analysis of phosphorylated ERK 1, 2 compared to total expression of ERK 1, 2. All analyses were performed 7 days after CLP.
A-F: no significant difference in t-test

4.4 Single-cell RNA sequencing of cardiac macrophages

In the single-cell RNA sequencing of leukocytes, the analysis especially focuses on cardiac macrophages (Figure 4.9, A). In cardiac macrophages two new clusters appear after CLP compared to control: Cluster 5 and 7. On the other hand, one cluster that is present in control mice is not present after CLP: Cluster 8. All other clusters are present in both groups (Figure 4.9, B, E).

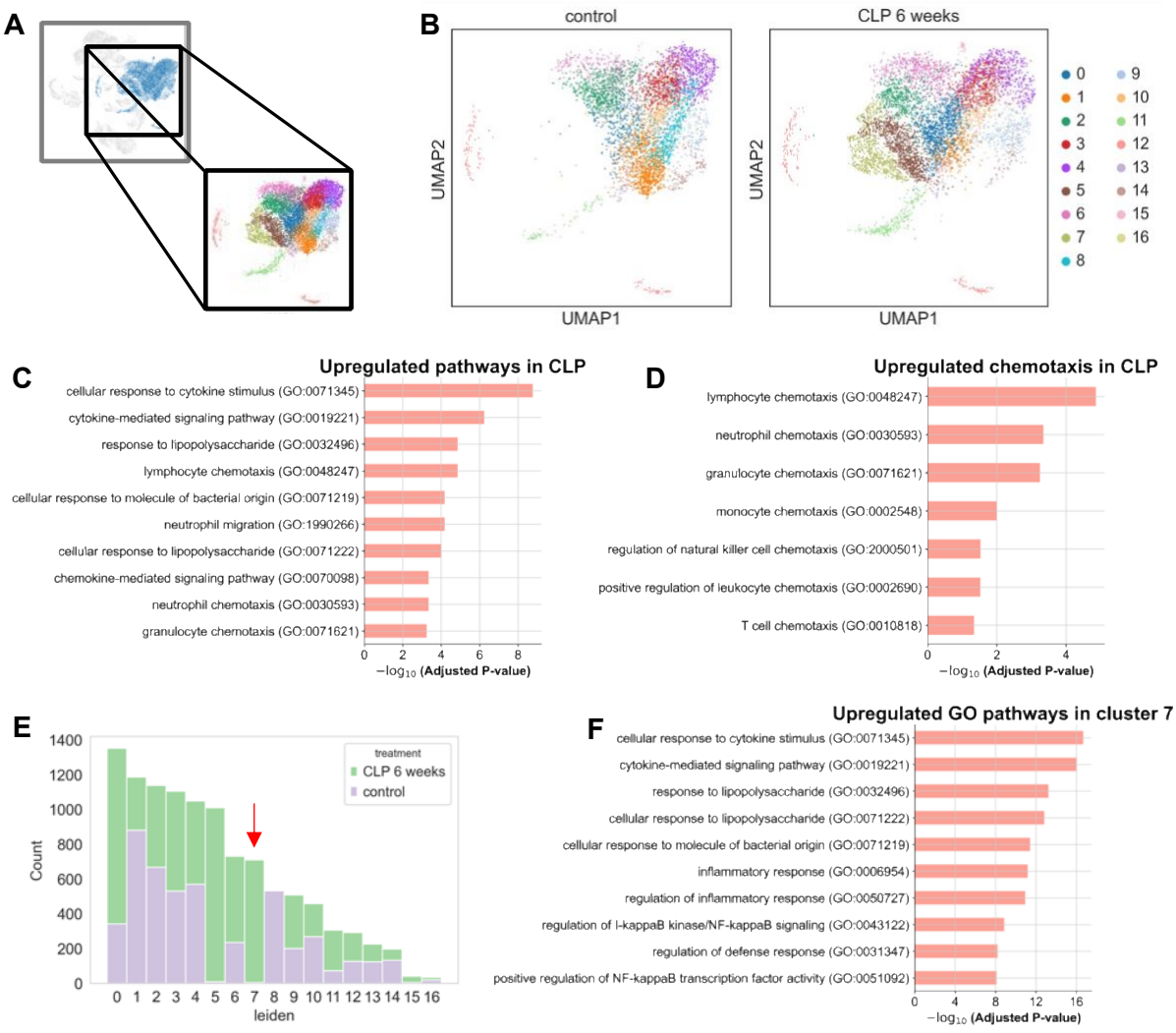

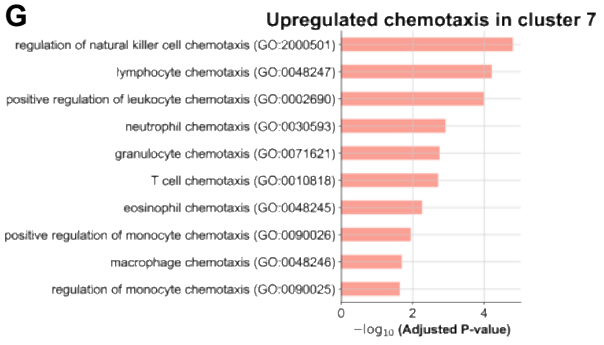

Figure 4.9: Chemotaxis pathways are upregulated in macrophages 6 weeks after CLP.
Single-cell RNA sequencing analysis of cardiac CD45-positive cells (leukocytes) 6 weeks after CLP and control.
UMAP of all CD45-positive cells, focused on macrophages (A), UMAP clusters of macrophages in control and CLP (B), pathways enrichment analysis of macrophages after CLP (C, D), cell count in Leiden clusters in CLP and control I, pathway enrichment analysis of cluster 7 (F, G).

After CLP the enrichment analysis defines several pathways that are upregulated: The most upregulated pathways are the cellular response to cytokine stimulus, the cytokine-mediated signaling and the response to lipopolysaccharide pathway (Figure 4.9, C). Additionally, chemotaxis of leukocytes is upregulated (Figure 4.9, D). Analyzing only Cluster 7 the same pathways are enriched, and chemotaxis is upregulated, too (Figure 4.9, F, G). In cluster 5, mitochondrial pathways are upregulated (Supplementary Figure 7.4.2).

Looking at specific genes, the genes Socs3, S100a9, S100a8, Ccl2, Ccl12, IL-1β and Cxcl2 are upregulated after CLP (Figure 4.10, A). These upregulations are mainly located in Cluster 7 (Figure 4.10: **Different genes are upregulated in macrophages 6 weeks after CLP.**

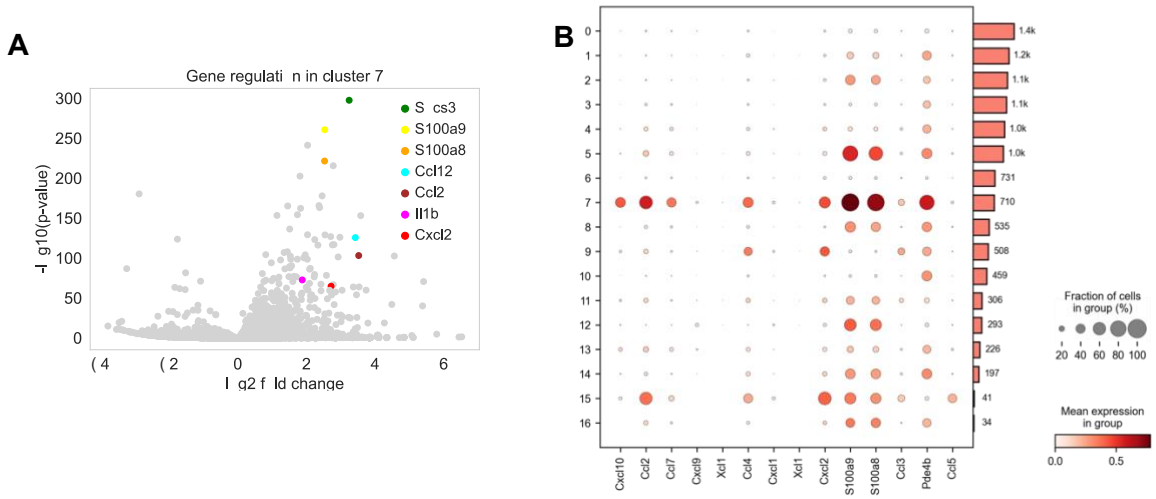

Figure 4.10: Different genes are upregulated in macrophages 6 weeks after CLP.
Single-cell RNA sequencing analysis of cardiac CD45-positive cells (leukocytes) 6 weeks after CLP and control.
Upregulated genes in CLP vs. control in cluster 7 (A), heat map of gene expression in Leiden clusters (B)

5. Discussion

5.1 Chronic effects of sepsis

As expected, CLP leads to an increase of white blood cell (WBC) count (Figure 4.2). In septic patients an increase of WBC count > 12000/mm^3 is part of the Systemic inflammatory response syndrome (SIRS) criteria that where formerly used to diagnose sepsis.[1] This leukocytosis is primarily driven by neutrophils, whose production and migration from the bone marrow to the infection site increases during severe infection.[16,17,87] The neutrophilia normalizes after about 7 weeks (Figure 4.2). Lymphopenia, resulting from the apoptosis of B- and T-lymphocytes, is common in sepsis and associated with poor outcomes.[24,25,88] In our model, however, lymphocyte count is not altered after sepsis (Figure 4.2). This is likely due to the timepoint of 1 week after CLP, as lymphopenia observed by Ammer-Herrmenau et al. day 3 after sepsis had already recovered on day 8.[89] Another possible explanation is that there are differences in the severity of sepsis due to minor differences in the experimental set up of the CLP model.

At baseline, the WBC count and the absolute values of neutrophils and lymphocytes show no significant difference between male and female mice, but relative neutrophil count and variance between individuals is significantly higher in male mice (Figure 4.3). This contrasts with human data, where neutrophil counts are higher in women and lymphocyte counts are higher in men.[90,91] One explanation for this discrepancy might be the group housing of male mice in laboratories. Male mice, even when housed exclusively with littermates, often exhibit aggressive behavior.[92] This can lead to fights and minor injuries, prompting an increase of blood neutrophils. This would hypothetically also explain the higher variability of neutrophil counts among male mice. Nonetheless, we monitored mice closely, and did not detect injuries in mice used for this experiment. Additionally, individual housing of males does not resolve this issue, as isolation also negatively affects the well-being of mice.[93]

One week after CLP, there is no significant difference in blood cell counts between male and female mice (Figure 4.3). Most studies on sex differences in response to sepsis indicate better survival rates and cardiac function of female mice during early sepsis.[94–97] However, Bojalil et al. saw no survival differences after CLP and human data on sex-based differences in sepsis is contradictory.[98,99] The other experiments of this thesis were performed with both male and female mice, with no further investigation into sex-based differences.

5.2 Sepsis does not lead to chronic changes in murine heart function and morphology.

For the first hypothesis of this thesis the hypothesis H0 can be confirmed: Sepsis does not lead to chronic changes in murine heart function. Neither systolic nor diastolic heart function is altered after CLP.

For the second hypothesis of this thesis the hypothesis H0 can be confirmed: Sepsis does not lead to chronic changes in murine heart morphology. No signs for cardiac hypertrophy or fibrosis are found seven weeks after CLP.

It is well established that sepsis leads to acute systolic and diastolic cardiac dysfunction which is associated with worse prognosis.[100–102] In mice, CLP also leads to impaired systolic and diastolic function during the first 96 hours.[103–106] However, this cardiac dysfunction in early sepsis is reversible, consistent with our findings of no impairment in cardiac function seven weeks after CLP (Figure 4.4, Figure 4.5).[107–110] Similarly, Shiji Wang et al. analyzed cardiac function eight weeks after CLP and saw in accordance with our results no difference in Ejection Fraction.[111] On the other hand, in their study fractional shortening was decreased after CLP and blood levels of BNP were increased.[111] In our model neither the fractional shortening seven weeks after CLP (Supplementary Figure 7.4.3) nor the cardiac BNP expression seven days nor eight weeks after CLP are altered significantly (Figure 4.4). These differences may be, again, due to minor differences in experimental set up. Our findings are in line with Zhang et al., who also see no decrease of fractional shortening or elevation of BNP expression 21 days after CLP.[110]

Regarding cardiac hypertrophy, Shiji Wang et al. observed an elevated heart weight and qualitative morphological changes of myocytes in HE staining eight weeks after CLP.[111] There is also evidence that LPS induction increases cardiomyocyte cross-sectional area.[112] We do not see any signs of cardiac hypertrophy seven weeks after CLP, the heart weight and the cardiomyocyte cross section are not altered compared to control (Figure 4.6). This is in line with results of Lina Zhang et al. who reported that initial morphologic changes in hearts 24 hours after CLP are no longer detectable 30 days after CLP.[113] Again, a possible explanation for the different findings is a variance in disease severity due to differences of the CLP model.

Immediately after CLP (18 hours or 48 hours), the collagen fraction and fibrotic area is increased in rodents and LPS induction over four weeks leads to cardiac fibrosis.[103,112,114] Additionally, in late sepsis – 12 days after CLP – cardiac fibrosis and the expression of fibrotic pathway genes, for example Tgf-β, are increased.[115] In our model we do not see any differences, as fibrotic genes are not upregulated in heart tissue seven days after CLP. Furthermore, we do not see an increase in

fibrotic area seven weeks after CLP (Figure 4.7, Figure 4.8). The only indication for cardiac fibrosis is an increase of Collagen type 3α1 expression 8 weeks after CLP (Figure 4.7). This discrepancy could be explained again by differences in disease severity due to variability of experimental factors such as length of ligated intestine or different needle sizes used for punction.[103,115] Haiju Zhang et al. for example ligate 1 cm of the cecum which also reflects in higher mortality compared to our model with 0.5 cm ligation length.[115] A less severe inflammatory response to CLP could explain why we do not see chronic functional or morphological changes in the myocardium.

5.3 Sepsis chronically impacts the macrophage milieu of the murine heart.

The third hypothesis of this thesis can be confirmed: Sepsis leads to chronic changes in the macrophage milieu of the murine heart.

It is already established that sepsis influences the macrophage population in the murine heart post-sepsis: Hoyer et al. observe a decrease in the number of cardiac macrophages one day after CLP, followed by an increase for 28 days. The increase is due to both, the recruitment of circulating monocytes to the heart and the proliferation of cardiac resident macrophages.[116]

Additionally, alterations of cardiac macrophages are observed in several studies after CLP. Genes involved in cell adhesion, immune system processes, inflammatory response and positive regulation of cell migration are enriched shortly after CLP, among them S100A9, CXCR2 and CXCL1.[117] Macrophage production of cytokines like IL-10 is increased, and they thereby contribute to the protection against myocardial damage in sepsis.[116,118] In another interesting study, single-cell RNA sequencing of cardiac macrophages three, seven and 21 days after CLP reveals a macrophage subcluster with high expression of TREM2 (Triggering receptor expressed on myeloid cells 2). This receptor is important for recovery of cardiomyocytes after sepsis, too.[110]

In our study, the macrophage expression profile notably shifts after CLP. Inflammatory pathways that mediate responses to cytokines, lipopolysaccharides, and leukocyte chemotaxis are significantly upregulated (Figure 4.9).

Furthermore, we identify a macrophage cluster present exclusively after CLP. This cluster is characterized by the expression of several inflammation-related cytokine genes, such as SOCS3, S100A8, S100A9, CCL12, CCL2, Il-1β and CXCL2 (Figure 4.10).

This is in line with findings of various studies showing an influence of sepsis on these cytokines: SOCS3 is known to be upregulated in circulating macrophages and neutrophils post-CLP.[119,120] CCL12 and CCL2, too, are upregulated in the central nervous system after CLP and chronic LPS-challenge increases CCL12 production.[67,116,121]

Additionally, certain cytokines have been linked to cardiac dysfunction after sepsis. Busch et al. observe that IL-1β contributes to sepsis-induced cardiomyopathy 24 hours after CLP.[105] In patients, S100A8 and S100A9 remain increased for months after sepsis, which is associated with cardiac dysfunction.[122,123] Both studies assess cardiac function during the acute phase of sepsis (24 hours after CLP or within 36 hours after admission to hospital).[105,123] While we also detect an upregulation of IL-1β, S100A8 and S100A9 in the macrophage cluster, we do not see associated cardiac dysfunction (Figure 4.4, Figure 4.5). A possible explanation for this discrepancy could be the timing, as sepsis-induced cardiomyopathy during the acute septic phase may be reversible.[109,110]

Changes in macrophage phenotype play a critical role in the development of cardiovascular dysfunction, particularly in the context of sepsis.[124,125] Macrophage polarization refers to the spectrum of activation states ranging from pro-inflammatory M1 macrophages to anti-inflammatory M2 macrophages.[126] An imbalance favoring pro-inflammatory polarization in cardiac resident macrophages can lead to chronic inflammation, myocardial fibrosis and hypertrophy, and heart failure.[127]

In our study, CLP induces a new cluster of cardiac macrophages characterized by the expression of cytokines associated with cardiac dysfunction. Although we did not observe any overt changes in cardiac function or morphology, these macrophages may still exert functional effects, for instance by altering the response to a subsequent myocardial injury.

A deeper understanding of this macrophage cluster and its functional consequences could support the development of targeted therapies aimed at preventing or mitigating cardiac dysfunction.

5.4 Limitations

This study provides important insights into the long-term effects of sepsis on the murine heart, particularly regarding the cardiac macrophage milieu. However, several limitations must be acknowledged.

A limitation is the lack of direct microbiological verification of sepsis. No blood cultures or other methods were used to confirm bacteremia or the systemic spread

of infection following CLP. Although the CLP model is well-established, the absence of culture-based confirmation limits the ability to precisely characterize the infectious component of the disease

In this study, animals received only analgesic treatment post-CLP. No antimicrobial or supportive therapies—such as fluid resuscitation or vasopressors—were administered. This represents a significant deviation from clinical reality, where human patients with sepsis typically receive prompt intensive care, including broad-spectrum antibiotics and organ support. As a result, the translational relevance of the findings may be limited, especially regarding the applicability to human patients receiving standard care.

The CLP model is sensitive to various technical factors—such as needle size, ligation length, and surgical technique—that can influence the severity of the septic insult. These variables may account for some discrepancies between this and other studies.

A central limitation is the absence of an assessment of macrophage polarization. While the study identifies changes in gene expression and cytokine profiles in heart-resident macrophages, it does not distinguish between M1-like and M2-like macrophage activation states. This restricts the ability to fully interpret the functional roles of macrophages post-sepsis, especially in the context of chronic inflammation, tissue remodeling, or resolution of injury. Including polarization markers or functional assays in future studies would allow for a more nuanced understanding of immune regulation and could help identify specific therapeutic targets.

Addressing these limitations in future studies will be essential for improving the clinical relevance and mechanistic insight into post-septic cardiac remodeling and immune regulation.

5.5 Conclusion

To conclude, the major finding of this thesis is that sublethal sepsis persistently changes cardiac macrophages. After recovery of sepsis a distinct inflammatory macrophage population is present in the murine heart. Further research is required to assess this population’s relevance in cardiovascular pathologies.

6. References

1 Singer M, Deutschman CS, Seymour CW, *et al.* The Third International Consensus Definitions for Sepsis and Septic Shock (Sepsis-3). *JAMA* 2016; **315**: 801–10.

2 Rudd KE, Johnson SC, Agesa KM, *et al.* Global, regional, and national sepsis incidence and mortality, 1990-2017: analysis for the Global Burden of Disease Study. *Lancet* 2020; **395**: 200–11.

3 Evans L, Rhodes A, Alhazzani W, *et al.* Surviving Sepsis Campaign: International Guidelines for Management of Sepsis and Septic Shock 2021. *Crit Care Med* 2021; **49**: e1063–143.

4 Gauer R, Forbes D, Boyer N. Sepsis: Diagnosis and Management. *afp* 2020; **101**: 409–18.

5 Prescott HC, Langa KM, Liu V, Escobar GJ, Iwashyna TJ. Increased 1-Year Healthcare Use in Survivors of Severe Sepsis. *Am J Respir Crit Care Med* 2014; **190**: 62–9.

6 Angriman F, Rosella LC, Lawler PR, Ko DT, Wunsch H, Scales DC. Sepsis hospitalization and risk of subsequent cardiovascular events in adults: a population-based matched cohort study. *Intensive Care Med* 2022; **48**: 448–57.

7 Yende S, Linde-Zwirble W, Mayr F, Weissfeld LA, Reis S, Angus DC. Risk of Cardiovascular Events in Survivors of Severe Sepsis. *Am J Respir Crit Care Med* 2014; **189**: 1065–74.

8 Ou S-M, Chu H, Chao P-W, *et al.* Long-Term Mortality and Major Adverse Cardiovascular Events in Sepsis Survivors. A Nationwide Population-based Study. *Am J Respir Crit Care Med* 2016; **194**: 209–17.

9 Jentzer JC, Lawler PR, Van Houten HK, Yao X, Kashani KB, Dunlay SM. Cardiovascular Events Among Survivors of Sepsis Hospitalization: A Retrospective Cohort Analysis. *J Am Heart Assoc* 2023; **12**: e027813.

10 Dalager-Pedersen M, Søgaard M, Schønheyder HC, Nielsen H, Thomsen RW. Risk for Myocardial Infarction and Stroke After Community-Acquired Bacteremia. *Circulation* 2014; **129**: 1387–96.

11 Wu M-H, Tsou P-Y, Wang Y-H, *et al.* Impact of post-sepsis cardiovascular complications on mortality in sepsis survivors: a population-based study. *Crit Care* 2019; **23**: 293.

12 Jafarzadeh SR, Thomas BS, Warren DK, Gill J, Fraser VJ. Longitudinal Study of the Effects of Bacteremia and Sepsis on 5-year Risk of Cardiovascular Events. *Clinical Infectious Diseases* 2016; **63**: 495–500.

13 Kosyakovsky LB, Angriman F, Katz E, *et al.* Association between sepsis survivorship and long-term cardiovascular outcomes in adults: a systematic review and meta-analysis. *Intensive Care Med* 2021; **47**: 931–42.

14 Takeuchi O, Akira S. Pattern Recognition Receptors and Inflammation. *Cell* 2010; **140**: 805–20.

15 Osuchowski MF, Welch K, Siddiqui J, Remick DG. Circulating Cytokine/Inhibitor Profiles Reshape the Understanding of the SIRS/CARS Continuum in Sepsis and Predict Mortality1. *The Journal of Immunology* 2006; **177**: 1967–74.

16 De Filippo K, Henderson RB, Laschinger M, Hogg N. Neutrophil chemokines KC and macrophage-inflammatory protein-2 are newly synthesized by tissue macrophages using distinct TLR signaling pathways. *J Immunol* 2008; **180**: 4308–15.

17 Brinkmann V, Reichard U, Goosmann C, *et al.* Neutrophil Extracellular Traps Kill Bacteria. *Science* 2004; **303**: 1532–5.

18 Czaikoski PG, Mota JMSC, Nascimento DC, *et al.* Neutrophil Extracellular Traps Induce Organ Damage during Experimental and Clinical Sepsis. *PLoS One* 2016; **11**: e0148142.

19 Nedeva C. Inflammation and Cell Death of the Innate and Adaptive Immune System during Sepsis. *Biomolecules* 2021; **11**: 1011.

20 Arora J, Mendelson AA, Fox-Robichaud A. Sepsis: network pathophysiology and implications for early diagnosis. *Am J Physiol Regul Integr Comp Physiol* 2023; **324**: R613–24.

21 Shao Z, Nishimura T, Leung LLK, Morser J. Carboxypeptidase B2 deficiency reveals opposite effects of complement C3a and C5a in a murine polymicrobial sepsis model. *J*

Thromb Haemost 2015; **13**: 1090–102.
22 Hotchkiss RS, Monneret G, Payen D. Sepsis-induced immunosuppression: from cellular dysfunctions to immunotherapy. *Nat Rev Immunol* 2013; **13**: 862–74.
23 Boomer JS, To K, Chang KC, *et al.* Immunosuppression in Patients Who Die of Sepsis and Multiple Organ Failure. *JAMA* 2011; **306**: 2594–605.
24 Drewry AM, Samra N, Skrupky LP, Fuller BM, Compton SM, Hotchkiss RS. Persistent Lymphopenia after Diagnosis of Sepsis Predicts Mortality. *Shock* 2014; **42**: 383–91.
25 Hotchkiss RS, Tinsley KW, Swanson PE, *et al.* Sepsis-Induced Apoptosis Causes Progressive Profound Depletion of B and CD4+ T Lymphocytes in Humans1. *The Journal of Immunology* 2001; **166**: 6952–63.
26 Hotchkiss RS, Tinsley KW, Swanson PE, *et al.* Depletion of Dendritic Cells, But Not Macrophages, in Patients with Sepsis. *The Journal of Immunology* 2002; **168**: 2493–500.
27 Voll RE, Herrmann M, Roth EA, Stach C, Kalden JR, Girkontaite I. Immunosuppressive effects of apoptotic cells. *Nature* 1997; **390**: 350–1.
28 Xue M, Xie J, Liu L, *et al.* Early and dynamic alterations of Th2/Th1 in previously immunocompetent patients with community-acquired severe sepsis: a prospective observational study. *J Transl Med* 2019; **17**: 57.
29 Cheng S-C, Scicluna BP, Arts RJW, *et al.* Broad defects in the energy metabolism of leukocytes underlie immunoparalysis in sepsis. *Nat Immunol* 2016; **17**: 406–13.
30 Rubio I, Osuchowski MF, Shankar-Hari M, *et al.* Current gaps in sepsis immunology: new opportunities for translational research. *The Lancet Infectious Diseases* 2019; **19**: e422–36.
31 Lajqi T, Köstlin-Gille N, Bauer R, *et al.* Training vs. Tolerance: The Yin/Yang of the Innate Immune System. *Biomedicines* 2023; **11**. DOI:10.3390/biomedicines11030766.
32 Netea MG, Quintin J, van der Meer JWM. Trained immunity: a memory for innate host defense. *Cell Host Microbe* 2011; **9**: 355–61.
33 Rieckmann A, Villumsen M, Sørup S, *et al.* Vaccinations against smallpox and tuberculosis are associated with better long-term survival: a Danish case-cohort study 1971–2010. *Int J Epidemiol* 2017; **46**: 695–705.
34 Giamarellos-Bourboulis EJ, Tsilika M, Moorlag S, *et al.* Activate: Randomized Clinical Trial of BCG Vaccination against Infection in the Elderly. *Cell* 2020; **183**: 315-323.e9.
35 Kleinnijenhuis J, Quintin J, Preijers F, *et al.* Bacille Calmette-Guérin induces NOD2-dependent nonspecific protection from reinfection via epigenetic reprogramming of monocytes. *Proc Natl Acad Sci U S A* 2012; **109**: 17537–42.
36 Cheng S-C, Quintin J, Cramer RA, *et al.* mTOR- and HIF-1α-mediated aerobic glycolysis as metabolic basis for trained immunity. *Science* 2014; **345**: 1250684.
37 Arts RJW, Novakovic B, Ter Horst R, *et al.* Glutaminolysis and Fumarate Accumulation Integrate Immunometabolic and Epigenetic Programs in Trained Immunity. *Cell Metab* 2016; **24**: 807–19.
38 Zhao S, Zhong Y, Fu X, *et al.* H3K4 Methylation Regulates LPS-Induced Proinflammatory Cytokine Expression and Release in Macrophages. *Shock* 2019; **51**: 401–6.
39 López-Collazo E, del Fresno C. Pathophysiology of endotoxin tolerance: mechanisms and clinical consequences. *Crit Care* 2013; **17**: 242.
40 Grondman I, Arts RJW, Koch RM, *et al.* Frontline Science: Endotoxin-induced immunotolerance is associated with loss of monocyte metabolic plasticity and reduction of oxidative burst. *J Leukoc Biol* 2019; **106**: 11–25.
41 Davis FM, Schaller MA, denDekker A, *et al.* Sepsis Induces Prolonged MLL1-mediated Epigenetic Modifications in Bone Marrow and Peripheral Macrophages Impairing Inflammation and Wound Healing. *Arterioscler Thromb Vasc Biol* 2019; **39**: 2353–66.
42 Lee MJ, Bae J, Lee JH, *et al.* Serial Change of Endotoxin Tolerance in a Polymicrobial Sepsis Model. *Int J Mol Sci* 2022; **23**: 6581.
43 Pena OM, Hancock DG, Lyle NH, *et al.* An Endotoxin Tolerance Signature Predicts Sepsis and Organ Dysfunction at Initial Clinical Presentation. *EBioMedicine* 2014; **1**: 64–71.
44 Induction of endotoxin tolerance enhances bacterial clearance and survival in murine polymicrobial sepsis - PubMed. https://pubmed.ncbi.nlm.nih.gov/18197145/ (accessed June 29, 2023).

45 Lehner MD, Ittner J, Bundschuh DS, van Rooijen N, Wendel A, Hartung T. Improved innate immunity of endotoxin-tolerant mice increases resistance to Salmonella enterica serovar typhimurium infection despite attenuated cytokine response. *Infect Immun* 2001; **69**: 463–71.
46 Hill AW, Shears AL, Hibbitt KG. Increased antibacterial activity against Escherichia coli in bovine serum after the induction of endotoxin tolerance. *Infect Immun* 1976; **14**: 257–65.
47 Maitra U, Deng H, Glaros T, *et al.* Molecular mechanisms responsible for the selective and low-grade induction of proinflammatory mediators in murine macrophages by lipopolysaccharide. *J Immunol* 2012; **189**: 1014–23.
48 Chen K, Geng S, Yuan R, Diao N, Upchurch Z, Li L. Super-low dose endotoxin pre-conditioning exacerbates sepsis mortality. *EBioMedicine* 2015; **2**: 324–33.
49 Li X, Wang H, Yu X, *et al.* Maladaptive innate immune training of myelopoiesis links inflammatory comorbidities. *Cell* 2022; **185**: 1709-1727.e18.
50 Machiels B, Dourcy M, Xiao X, *et al.* A gammaherpesvirus provides protection against allergic asthma by inducing the replacement of resident alveolar macrophages with regulatory monocytes. *Nat Immunol* 2017; **18**: 1310–20.
51 Jeyanathan M, Vaseghi-Shanjani M, Afkhami S, *et al.* Parenteral BCG vaccine induces lung-resident memory macrophages and trained immunity via the gut–lung axis. *Nat Immunol* 2022; **23**: 1687–702.
52 Dejager L, Pinheiro I, Dejonckheere E, Libert C. Cecal ligation and puncture: the gold standard model for polymicrobial sepsis? *Trends in Microbiology* 2011; **19**: 198–208.
53 Wang N, Lu Y, Zheng J, Liu X. Of mice and men: Laboratory murine models for recapitulating the immunosuppression of human sepsis. *Front Immunol* 2022; **13**: 956448.
54 Vincent J-L, Rello J, Marshall J, *et al.* International study of the prevalence and outcomes of infection in intensive care units. *JAMA* 2009; **302**: 2323–9.
55 Wolpe SD, Sherry B, Juers D, Davatelis G, Yurt RW, Cerami A. Identification and characterization of macrophage inflammatory protein 2. *Proc Natl Acad Sci U S A* 1989; **86**: 612–6.
56 Liu S, Liu J, Yang X, *et al.* Cis-acting lnc-Cxcl2 restrains neutrophil-mediated lung inflammation by inhibiting epithelial cell CXCL2 expression in virus infection. *Proc Natl Acad Sci U S A* 2021; **118**: e2108276118.
57 Lentini G, Famà A, Biondo C, *et al.* Neutrophils Enhance Their Own Influx to Sites of Bacterial Infection via Endosomal TLR-Dependent Cxcl2 Production. *J Immunol* 2020; **204**: 660–70.
58 Li JL, Lim CH, Tay FW, *et al.* Neutrophils Self-Regulate Immune Complex-Mediated Cutaneous Inflammation through CXCL2. *J Invest Dermatol* 2016; **136**: 416–24.
59 Eash KJ, Greenbaum AM, Gopalan PK, Link DC. CXCR2 and CXCR4 antagonistically regulate neutrophil trafficking from murine bone marrow. *J Clin Invest* 2010; **120**: 2423–31.
60 Christopher MJ, Liu F, Hilton MJ, Long F, Link DC. Suppression of CXCL12 production by bone marrow osteoblasts is a common and critical pathway for cytokine-induced mobilization. *Blood* 2009; **114**: 1331–9.
61 Wengner AM, Pitchford SC, Furze RC, Rankin SM. The coordinated action of G-CSF and ELR + CXC chemokines in neutrophil mobilization during acute inflammation. *Blood* 2008; **111**: 42–9.
62 Bajrami B, Zhu H, Kwak H-J, *et al.* G-CSF maintains controlled neutrophil mobilization during acute inflammation by negatively regulating CXCR2 signaling. *J Exp Med* 2016; **213**: 1999–2018.
63 McDonald B, Pittman K, Menezes GB, *et al.* Intravascular Danger Signals Guide Neutrophils to Sites of Sterile Inflammation. *Science* 2010; **330**: 362–6.
64 Sadik CD, Kim ND, Luster AD. Neutrophils cascading their way to inflammation. *Trends Immunol* 2011; **32**: 452–60.
65 Hoyer FF, Naxerova K, Schloss MJ, *et al.* Tissue-Specific Macrophage Responses to Remote Injury Impact the Outcome of Subsequent Local Immune Challenge. *Immunity* 2019; **51**: 899-914.e7.
66 Kaynar AM, Yende S, Zhu L, *et al.* Effects of intra-abdominal sepsis on atherosclerosis in mice. *Crit Care* 2014; **18**: 469.

67 Singer BH, Newstead MW, Zeng X, *et al.* Cecal Ligation and Puncture Results in Long-Term Central Nervous System Myeloid Inflammation. *PLOS ONE* 2016; **11**: e0149136.
68 Abraham MN, Kelly AP, Brandwein AB, *et al.* USE OF ORGAN DYSFUNCTION AS A PRIMARY OUTCOME VARIABLE FOLLOWING CECAL LIGATION AND PUNCTURE: RECOMMENDATIONS FOR FUTURE STUDIES. *Shock* 2020; **54**: 168–82.
69 Vandewalle J, Steeland S, Van Ryckeghem S, *et al.* A Study of Cecal Ligation and Puncture-Induced Sepsis in Tissue-Specific Tumor Necrosis Factor Receptor 1-Deficient Mice. *Front Immunol* 2019; **10**: 2574.
70 Nullens S, De Man J, Bridts C, Ebo D, Francque S, De Winter B. Identifying Therapeutic Targets for Sepsis Research: A Characterization Study of the Inflammatory Players in the Cecal Ligation and Puncture Model. *Mediators Inflamm* 2018; **2018**: 5130463.
71 Ruiz S, Vardon-Bounes F, Merlet-Dupuy V, *et al.* Sepsis modeling in mice: ligation length is a major severity factor in cecal ligation and puncture. *Intensive Care Med Exp* 2016; **4**: 22.
72 Singleton KD, Wischmeyer PE. Distance of Cecum Ligated Influences Mortality, Tumor Necrosis Factor-Alpha and Interleukin-6 Expression following Cecal Ligation and Puncture in the Rat. *European Surgical Research* 2003; **35**: 486–91.
73 Hees Soler J. Bachelorthesis: Sepsis induzierte langfristige Veränderungen des myokardialen Makrophagen-Milieus. 2021; published online June 9.
74 Nagueh SF, Smiseth OA, Appleton CP, *et al.* Recommendations for the Evaluation of Left Ventricular Diastolic Function by Echocardiography: An Update from the American Society of Echocardiography and the European Association of Cardiovascular Imaging. *Journal of the American Society of Echocardiography* 2016; **29**: 277–314.
75 Sohn D-W, Chai I-H, Lee D-J, *et al.* Assessment of Mitral Annulus Velocity by Doppler Tissue Imaging in the Evaluation of Left Ventricular Diastolic Function. *Journal of the American College of Cardiology* 1997; **30**: 474–80.
76 Dandel M, Lehmkuhl H, Knosalla C, Suramelashvili N, Hetzer R. Strain and Strain Rate Imaging by Echocardiography – Basic Concepts and Clinical Applicability. *Curr Cardiol Rev* 2009; **5**: 133–48.
77 Luttmann W, Bratke K, Küpper M, Myrtek D. Der Experimentator: Immunologie. Berlin, Heidelberg: Springer Berlin Heidelberg, 2014 DOI:10.1007/978-3-642-41899-0.
78 Expression of leukocyte common antigen (CD45) on various human leukemia/lymphoma cell lines - PubMed. https://pubmed.ncbi.nlm.nih.gov/2140233/# (accessed Oct 14, 2023).
79 Rheinländer A, Schraven B, Bommhardt U. CD45 in human physiology and clinical medicine. *Immunol Lett* 2018; **196**: 22–32.
80 Jovic D, Liang X, Zeng H, Lin L, Xu F, Luo Y. Single-cell RNA sequencing technologies and applications: A brief overview. *Clin Transl Med* 2022; **12**: e694.
81 Slovin S, Carissimo A, Panariello F, *et al.* Single-Cell RNA Sequencing Analysis: A Step-by-Step Overview. *Methods Mol Biol* 2021; **2284**: 343–65.
82 The Ultimate Guide to t-tests. https://www.graphpad.com/guides/the-ultimate-guide-to-t-tests (accessed July 24, 2022).
83 GraphPad Prism 9 Statistics Guide - Analysis checklist: Two-way ANOVA. https://www.graphpad.com/guides/prism/latest/statistics/stat_checklist_2wayanova.htm (accessed Aug 11, 2022).
84 The Ultimate Guide to ANOVA. https://www.graphpad.com/guides/the-ultimate-guide-to-anova (accessed July 27, 2022).
85 Xu Z, Castellino FJ, Ploplis VA. Plasminogen activator inhibitor-1 (PAI-1) is cardioprotective in mice by maintaining microvascular integrity and cardiac architecture. *Blood* 2010; **115**: 2038–47.
86 Liu M, López de Juan Abad B, Cheng K. Cardiac fibrosis: Myofibroblast-mediated pathological regulation and drug delivery strategies. *Adv Drug Deliv Rev* 2021; **173**: 504–19.
87 Farkas JD. The complete blood count to diagnose septic shock. *J Thorac Dis* 2020; **12**: S16–21.
88 Cilloniz C, Peroni HJ, Gabarrús A, *et al.* Lymphopenia Is Associated With Poor Outcomes of Patients With Community-Acquired Pneumonia and Sepsis. *Open Forum Infect Dis* 2021; **8**: ofab169.
89 Ammer-Herrmenau C, Kulkarni U, Andreas N, *et al.* Sepsis induces long-lasting

impairments in CD4+ T-cell responses despite rapid numerical recovery of T-lymphocyte populations. *PLoS One* 2019; **14**: e0211716.
90 Abdullah M, Chai P-S, Chong M-Y, *et al.* Gender effect on in vitro lymphocyte subset levels of healthy individuals. *Cell Immunol* 2012; **272**: 214–9.
91 Bain BJ, England JM. Normal haematological values: sex difference in neutrophil count. *Br Med J* 1975; **1**: 306–9.
92 Weber EM, Dallaire JA, Gaskill BN, Pritchett-Corning KR, Garner JP. Aggression in group-housed laboratory mice: why can't we solve the problem? *Lab Anim (NY)* 2017; **46**: 157–61.
93 Kappel S, Hawkins P, Mendl MT. To Group or Not to Group? Good Practice for Housing Male Laboratory Mice. *Animals (Basel)* 2017; **7**: 88.
94 Zellweger R, Wichmann MW, Ayala A, Stein S, DeMaso CM, Chaudry IH. Females in proestrus state maintain splenic immune functions and tolerate sepsis better than males. *Critical Care Medicine* 1997; **25**: 106.
95 Drechsler S, Weixelbaumer K, Raeven P, *et al.* Relationship between Age/Gender-Induced Survival Changes and the Magnitude of Inflammatory Activation and Organ Dysfunction in Post-Traumatic Sepsis. *PLoS One* 2012; **7**: e51457.
96 Wehrenpfennig P, Drechsler S, Weixelbaumer KM, Bahrami S, Osuchowski MF. Mouse Model of Posttraumatic Abdominal Sepsis: Survival Advantage of Females over Males Does Not Depend on the Cecum Size. *European Surgical Research* 2014; **52**: 83–9.
97 Chen J, Chiazza F, Collino M, Patel NSA, Coldewey SM, Thiemermann C. Gender Dimorphism of the Cardiac Dysfunction in Murine Sepsis: Signalling Mechanisms and Age-Dependency. *PLoS One* 2014; **9**: e100631.
98 Dias SP, Brouwer MC, van de Beek D. Sex and Gender Differences in Bacterial Infections. *Infect Immun*; **90**: e00283-22.
99 Bojalil R, Ruíz-Hernández A, Villanueva-Arias A, *et al.* Two murine models of sepsis: immunopathological differences between the sexes—possible role of TGFβ1 in female resistance to endotoxemia. *Biol Res* 2023; **56**: 54.
100 Wilhelm J, Hettwer S, Schuermann M, *et al.* Severity of cardiac impairment in the early stage of community-acquired sepsis determines worse prognosis. *Clin Res Cardiol* 2013; **102**: 735–44.
101 Lin Y, Xu Y, Zhang Z. Sepsis-Induced Myocardial Dysfunction (SIMD): the Pathophysiological Mechanisms and Therapeutic Strategies Targeting Mitochondria. *Inflammation* 2020; **43**: 1184–200.
102 Sanfilippo F, Corredor C, Fletcher N, *et al.* Diastolic dysfunction and mortality in septic patients: a systematic review and meta-analysis. *Intensive Care Med* 2015; **41**: 1004–13.
103 Zeng N, Jian Z, Xu J, Zheng S, Fan Y, Xiao F. DLK1 overexpression improves sepsis-induced cardiac dysfunction and fibrosis in mice through the TGF-β1/Smad3 signaling pathway and MMPs. *J Mol Histol* 2023; **54**: 655–64.
104 O'Riordan CE, Purvis GSD, Collotta D, *et al.* Bruton's Tyrosine Kinase Inhibition Attenuates the Cardiac Dysfunction Caused by Cecal Ligation and Puncture in Mice. *Frontiers in Immunology* 2019; **10**. https://www.frontiersin.org/articles/10.3389/fimmu.2019.02129 (accessed Nov 24, 2023).
105 Busch K, Kny M, Huang N, *et al.* Inhibition of the NLRP3/IL-1β axis protects against sepsis-induced cardiomyopathy. *J Cachexia Sarcopenia Muscle* 2021; **12**: 1653–68.
106 Hoffman M, Kyriazis ID, Lucchese AM, *et al.* Myocardial Strain and Cardiac Output are Preferable Measurements for Cardiac Dysfunction and Can Predict Mortality in Septic Mice. *J Am Heart Assoc* 2019; **8**: e012260.
107 Antonucci E, Fiaccadori E, Donadello K, Taccone FS, Franchi F, Scolletta S. Myocardial depression in sepsis: From pathogenesis to clinical manifestations and treatment. *Journal of Critical Care* 2014; **29**: 500–11.
108 Parker MM, Shelhamer JH, Bacharach SL, *et al.* Profound but reversible myocardial depression in patients with septic shock. *Ann Intern Med* 1984; **100**: 483–90.
109 Vallabhajosyula S, Jentzer JC, Geske JB, *et al.* New-Onset Heart Failure and Mortality in Hospital Survivors of Sepsis-Related Left Ventricular Dysfunction. *Shock* 2018; **49**: 144–9.
110 Zhang K, Wang Y, Chen S, *et al.* TREM2hi resident macrophages protect the septic

heart by maintaining cardiomyocyte homeostasis. *Nat Metab* 2023; **5**: 129–46.
111 Wang S, Wang G, Dong L, *et al.* The Overexpression of miR-377 Aggravates Sepsis-Induced Myocardial Hypertrophy by Binding to Rcan2 and Mediating CaN Activity. *Oxid Med Cell Longev* 2022; **2022**: 6659183.
112 Zhuang J, Chen L, Li G, *et al.* RCAN1 deficiency aggravates sepsis-induced cardiac remodeling and dysfunction by accelerating mitochondrial pathological fission. *Inflamm Res* 2022; **71**: 1589–602.
113 Zhang L, Qi D, Peng M, *et al.* Decoding molecular signature on heart of septic mice with distinct left ventricular ejection fraction. *iScience* 2023; **26**: 107825.
114 Zeng N, Xu J, Yao W, Li S, Ruan W, Xiao F. Brain-Derived Neurotrophic Factor Attenuates Septic Myocardial Dysfunction via eNOS/NO Pathway in Rats. *Oxid Med Cell Longev* 2017; **2017**: 1721434.
115 Zhang H, Caudle Y, Shaikh A, Yao B, Yin D. Inhibition of microRNA-23b prevents polymicrobial sepsis-induced cardiac dysfunction by modulating TGIF1 and PTEN. *Biomed Pharmacother* 2018; **103**: 869–78.
116 Hoyer FF, Naxerova K, Schloss MJ, *et al.* Tissue-Specific Macrophage Responses to Remote Injury Impact the Outcome of Subsequent Local Immune Challenge. *Immunity* 2019; **51**: 899-914.e7.
117 Yan X, Zhang Y-L, Han X, Li P-B, Guo S-B, Li H-H. Time Series Transcriptomic Analysis by RNA Sequencing Reveals a Key Role of PI3K in Sepsis-Induced Myocardial Injury in Mice. *Front Physiol* 2022; **13**: 903164.
118 Zou X-Z, Hao J-F, Hou M-X. Hmgcs2 regulates M2 polarization of macrophages to repair myocardial injury induced by sepsis. *Aging (Albany NY)* 2023; **15**: 7794–810.
119 DeMartini T, Nowell M, James J, *et al.* High fat diet-induced obesity increases myocardial injury and alters cardiac STAT3 signaling in mice after polymicrobial sepsis. *Biochim Biophys Acta Mol Basis Dis* 2017; **1863**: 2654–60.
120 Grutkoski PS, Chen Y, Chung CS, Ayala A. Sepsis-induced SOCS-3 expression is immunologically restricted to phagocytes. *J Leukoc Biol* 2003; **74**: 916–22.
121 DeLeon-Pennell KY, Iyer RP, Ero OK, *et al.* Periodontal-induced chronic inflammation triggers macrophage secretion of Ccl12 to inhibit fibroblast-mediated cardiac wound healing. *JCI Insight*; **2**: e94207.
122 Denstaedt SJ, Bustamante AC, Newstead MW, *et al.* Long-term survivors of murine sepsis are predisposed to enhanced LPS-induced lung injury and proinflammatory immune reprogramming. *Am J Physiol Lung Cell Mol Physiol* 2021; **321**: L451–65.
123 Jakobsson G, Papareddy P, Andersson H, *et al.* Therapeutic S100A8/A9 blockade inhibits myocardial and systemic inflammation and mitigates sepsis-induced myocardial dysfunction. *Crit Care* 2023; **27**: 374.
124 Yang P, Chen Z, Huang W, Zhang J, Zou L, Wang H. Communications between macrophages and cardiomyocytes. *Cell Communication and Signaling : CCS* 2023; **21**: 206.
125 Chen X, Liu Y, Gao Y, Shou S, Chai Y. The roles of macrophage polarization in the host immune response to sepsis. *Int Immunopharmacol* 2021; **96**: 107791.
126 Ruytinx P, Proost P, Van Damme J, Struyf S. Chemokine-Induced Macrophage Polarization in Inflammatory Conditions. *Front Immunol* 2018; **9**: 1930.
127 Kang M, Jia H, Feng M, *et al.* Cardiac macrophages in maintaining heart homeostasis and regulating ventricular remodeling of heart diseases. *Front Immunol* 2024; **15**: 1467089.

7. Appendix

7.1 List of Figures

Figure 3.1: Survival after CLP surgery according to ligation length 20
Figure 3.2: Procedure of CLP surgery 21

Figure 4.1: Experimental design 34
Figure 4.2: CLP induces neutrophilia for about 6 weeks. 35
Figure 4.3: The immune reaction to CLP is similar in female and male mice despite baseline differences. 36
Figure 4.4: Systolic heart function is not altered in mice 7 weeks after CLP compared to control. 37
Figure 4.5: Diastolic heart function is not worsened in mice 7 weeks after CLP compared to control. 38
Figure 4.6: CLP does not lead to cardiac hypertrophy. 40
Figure 4.7: CLP does not lead to fibrotic changes in the myocardium. 41
Figure 4.8: Fibrosis inducing pathways are not altered 7 days after CLP. 42
Figure 4.9: Chemotaxis pathways are upregulated in macrophages 6 weeks after CLP. 43
Figure 4.10: Different genes are upregulated in macrophages 6 weeks after CLP. 44

7.2 List of Tables

Table 3.1: Recipe for injection narcosis 19
Table 3.2: Protocol for qPCR (Taq®Man Assay) 23
Table 3.3: Protocol for qPCR (GoTaq® qPCR Master Mix) 24
Table 3.4: Primers used for qPCR. 24
Table 3.5: Antibodies used for Western Blots 26
Table 3.6: Excitation Peak and Emission Peak wavelengths for fluorophores used in this thesis 29
Table 3.7: Recipe for FACS digestion buffer 30
Table 3.8: List of fluorescence labeled antibodies used for flow cytometry. 30

7.3 Recipes

7.3.1. RIPA-Buffer

50mM Tris−HCl; pH=7.4

50mM NaCl

1% Triton X-100

0.5% (w/v) Sodium deoxycholate

0.1% (w/v) Sodium dodecyl sulfate (SDS)

1mM Ethylenediaminetetraacetic acid (EDTA)

7.3.2. 4x Laemmli Sample Buffer

126mM Tris; pH=6.8

40% Glycerin

8% SDS

0.04% Bromphenol blue

Added: Dithiothreitol (DTT) 50µl (1M)

7.3.3. 10x SDS-PAGE Running Buffer

Tris Base 30.2g

Glycin 144.0g

EDTA 7.44g

SDS 30ml (20% SDS)

Ad 1000 ml Aq. dest.

7.3.4. Transfer Buffer

Tris Base 4.545g

Glycin 21.6g

MetOH 300ml

SDS 7.5 ml (20% SDS)

Ad 1500 ml Aq. Dest

7.4 Supplementary Figures

7.4.1. Original Pictures WesternBlot

(1) Molecular weight marker

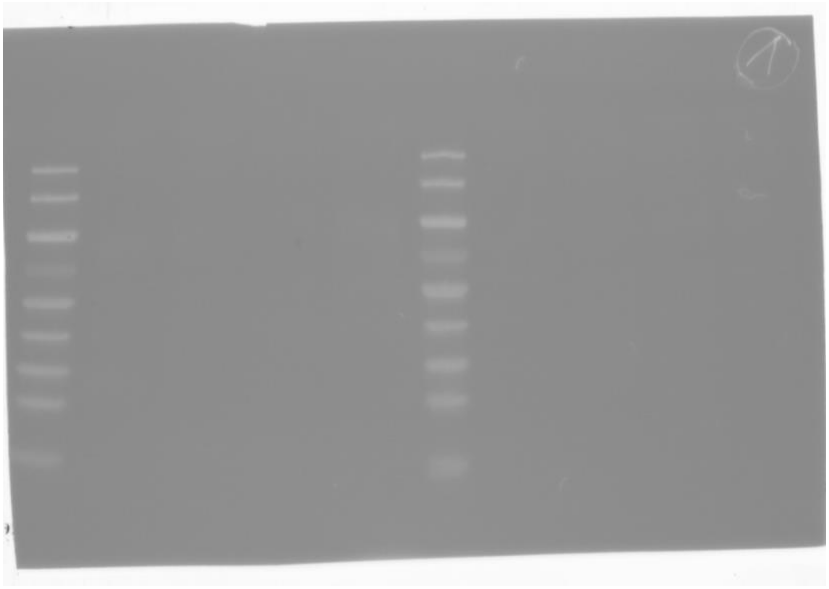

(2) pERK 1, 2

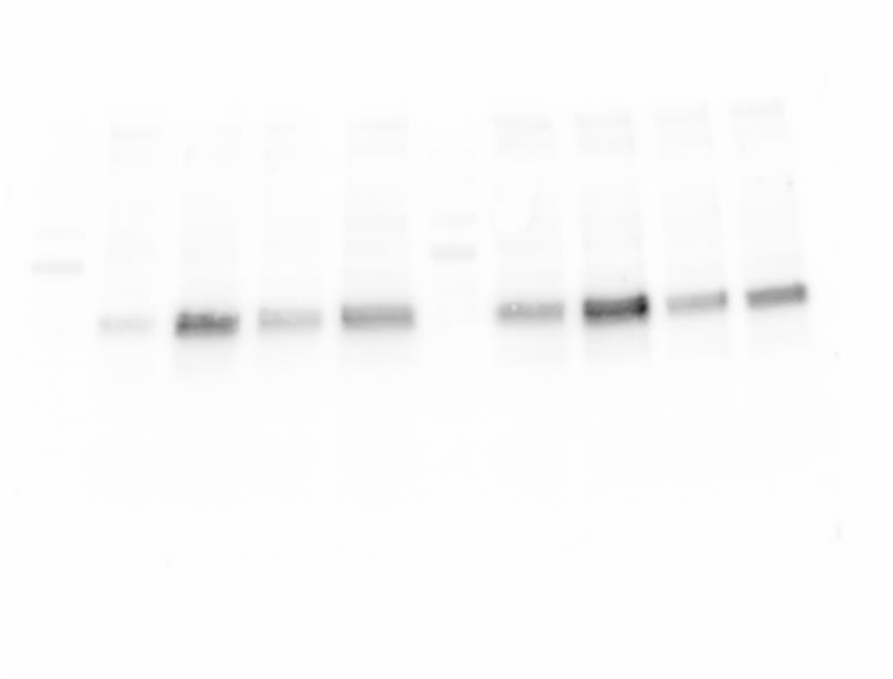

(3) ERK 1, 2

(4) GAPDH

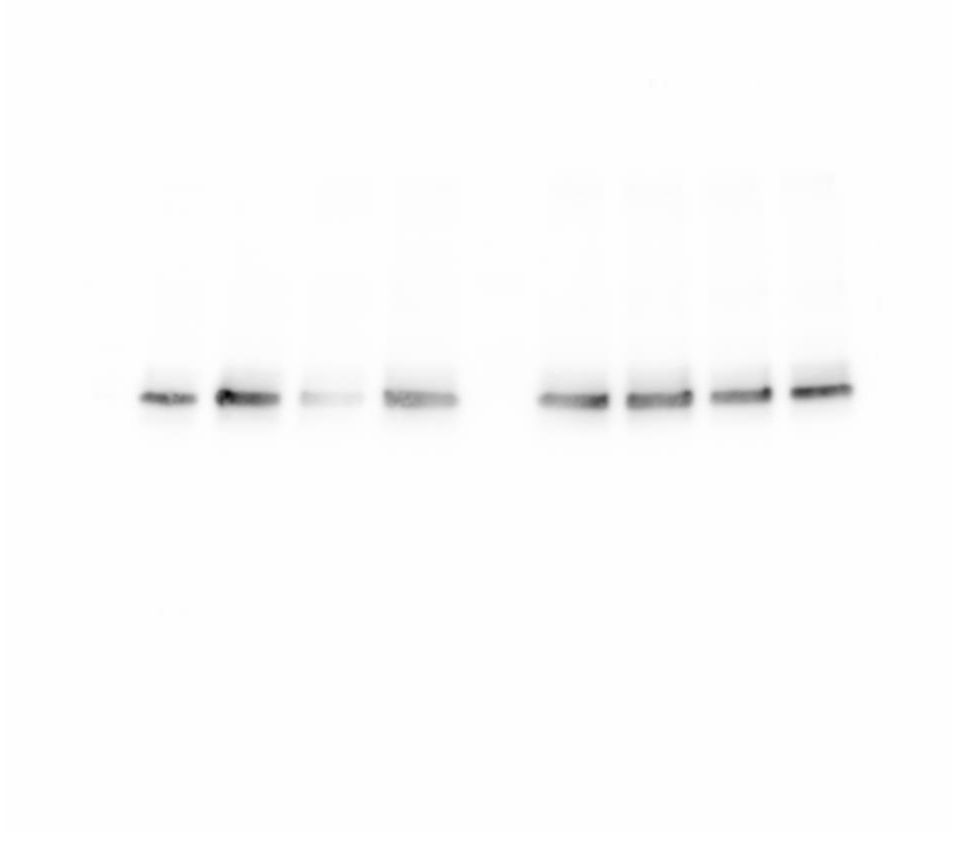

7.4.2. Pathways enrichment analysis of cluster 5

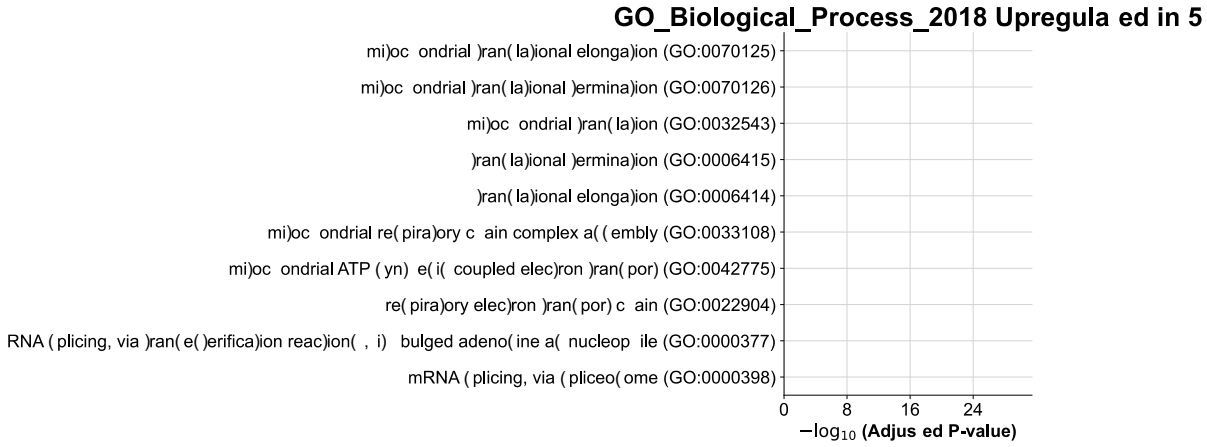

7.4.3. Unpaired samples t-test of Fractional Shortening 7 weeks after CLP

Group	7 weeks after CLP	control
Mean of Fractional shortening [%]	12.252	11.918
Standarddeviation	2.608	2.181
t-test	p=0.742	